

Copyright Warning & Restrictions

The copyright law of the United States (Title 17, United States Code) governs the making of photocopies or other reproductions of copyrighted material.

Under certain conditions specified in the law, libraries and archives are authorized to furnish a photocopy or other reproduction. One of these specified conditions is that the photocopy or reproduction is not to be “used for any purpose other than private study, scholarship, or research.” If a user makes a request for, or later uses, a photocopy or reproduction for purposes in excess of “fair use” that user may be liable for copyright infringement,

This institution reserves the right to refuse to accept a copying order if, in its judgment, fulfillment of the order would involve violation of copyright law.

Please Note: The author retains the copyright while the New Jersey Institute of Technology reserves the right to distribute this thesis or dissertation

Printing note: If you do not wish to print this page, then select “Pages from: first page # to: last page #” on the print dialog screen

The Van Houten library has removed some of the personal information and all signatures from the approval page and biographical sketches of theses and dissertations in order to protect the identity of NJIT graduates and faculty.

ABSTRACT

EXPERIMENTAL ION IMPLANTATION SYSTEM FOR DECABORANE IONS

**by
Vijay Babaram**

Future generations of Si technology will require ultra shallow junctions (tens of nm) in the drain and source regions of MOS transistors. Fabrication of such shallow p-type junctions requires implantation of boron at ultra low energies (< 1 keV), below the limits of standard ion implantation technology. A proposed solution involves implantation of $B_{10}H_x^+$ ions in which boron atoms carry less than 10 % of the beam energy.

This thesis is a part of the feasibility study of this new technology. An experimental ion implantation system was designed and built at Ion Beam and Thin Film Lab, NJIT. The system was tested and the mass analyzing magnet was calibrated using argon ions. Decaborane ions, of the order of microamperes, were successfully generated and implanted into Si. Beam-profiling experiments were performed to understand the shape of the beam and magnet focussing. Ion mass spectra of decaborane from the experimental implanter agreed with earlier measurements with a quadrupole mass spectrometer. The implanted boron dose was measured at Bell Labs, Murray Hill, NJ, using Nuclear Reaction Analysis (NRA). From electrostatic beam deflection experiments, it was concluded that there is no significant neutral beam component and no substantial breakup of $B_{10}H_x^+$ ions after the magnet. Boron dose determined from current integration with horizontal beam scan and electron suppression was within 7 % of the dose measured with NRA. The developed experimental ion implantation system will be used for investigating the characteristics of Si implanted with decaborane ions.

EXPERIMENTAL ION IMPLANTATION SYSTEM FOR DECABORANE IONS

by
Vijay Babaram

**A Thesis
Submitted to the Faculty of
New Jersey Institute of Technology
in Partial Fulfillment of the Requirements for the Degree of
Master of Science in Electrical Engineering**

Department of Electrical and Computer Engineering

January 2000

Blank Page

APPROVAL PAGE

EXPERIMENTAL ION IMPLANTATION SYSTEM FOR DECABORANE IONS

Vijay Babaram

Dr. Marek Sosnowski, Thesis Advisor / Date
Assoc. Professor, Department of Electrical and Computer Engineering, NJIT.

Dr. Haim Grebel, Committee Member / Date
Professor of Electrical Engineering, Department of Electrical and Computer Engineering,
NJIT.

Dr. John Poate, Committee Member Date
Department of Physics, NJIT.

Dr. Dale Jacobson, Committee Member Date
Bell Laboratories-Lucent Technologies, Murray Hill, NJ

BIOGRAPHICAL SKETCH

Author: Vijay Babaram
Degree: Master of Science
Date: January 2000

Undergraduate and Graduate Education:

- Master of Science in Electrical Engineering,
New Jersey Institute of Technology, Newark, NJ, 2000
- Bachelor of Engineering in Electronics and Communication Engineering,
Rashtreeya Vidyalaya College of Engineering, Bangalore, India, 1997

Major: Electrical Engineering

**This thesis is dedicated to my
beloved parents**

ACKNOWLEDGEMENT

Words fail to express my utmost sense of gratitude to Dr. Marek Sosnowski, who provided me with the wonderful opportunity of working under his supervision during my graduate study at NJIT, and served as my research advisor. I am extremely thankful to him not only for his deep sense of patience and understanding, but also for his expert guidance and invaluable suggestions, which encouraged and motivated me during every stage of my work.

I would also like to thank Dr. John Poate, Dr. Haim Grebel and Dr. Dale Jacobson for serving as members of the committee.

My fellow students at the Ion Beam and Thin Film Laboratory, Maria Albano and Anamika Patel are deserving of appreciation for their support. Special recognition also goes to Ed Oksienik for his help in machining components for the system.

TABLE OF CONTENTS

Chapter	Page
1. INTRODUCTION.....	1
2. EXPERIMENTAL ION IMPLANTATION SYSTEM.....	6
2.1 Ion Source.....	7
2.1.1 Construction and Operation.....	8
2.1.2 Simulation of the Ion Source.....	10
2.1.3 Notes on the Operation of the Ion Source.....	13
2.2 Mass Analyzing Magnet.....	14
2.2.1 Principle of Operation.....	14
2.2.2 Specifications.....	15
2.3 Sample Chamber and Deflection Plates.....	16
2.3.1 Sample Chamber.....	16
2.3.2 Deflection Plates.....	18
2.4 Description of Beamline, Vacuum and Gas Handling System.....	19
2.4.1 Beamline Section.....	19
2.4.2 Vacuum Foreline and Filter Section.....	22
2.4.3 Gas Handling System.....	22
3. EXPERIMENTS WITH ARGON AND MAGNET CALIBRATION.....	25
3.1 Ion Mass Spectrum of Argon and Calibration of Mass Analyzing Magnet	26
3.1.1 Ion Beam Spectrum.....	26
3.1.2 Calibration Graph and Ion Mass Spectrum.....	27

TABLE OF CONTENTS
(Continued)

Chapter	Page
3.2 Argon Ion Beam Profiling in the Horizontal Plane.....	30
3.2.1 Micrometer Beam Profiling in the Horizontal Plane.....	30
3.2.2 Beam Profiling by Magnetic Field Variation.....	30
3.2.3 Comparison of Micrometer and Magnet Scans.....	32
3.3 Argon Beam Profiling in the Vertical Plane.....	33
4. EXPERIMENTS WITH DECABORANE ION BEAM.....	35
4.1 Ionization of Decaborane and Decaborane Spectra.....	35
4.2 Integration of B ₁₀ Ion Current	38
4.3 Beam Profiling of Decaborane Ion Beam.....	40
4.4 Decaborane Implantation with Deflection and NRA.....	42
4.4.1 Electrostatic Deflection of Decaborane Beam and Implantation.	42
4.4.2 Nuclear Reaction Analysis and Results.....	43
4.5 Implantation Experiments with a Scanned Decaborane Beam.....	45
5. SUMMARY AND CONCLUSIONS.....	49
5.1 Experiments with Argon.....	50
5.2 Experiments with Decaborane.....	50
APPENDIX A DECABORANE.....	52
APPENDIX B MAGNET CONTROL AND DATA ACQUISITION SYSTEM USING A COMPUTER WITH LABVIEW™ SOFTWARE.....	55
B.1 Control Circuit for Magnet	56

TABLE OF CONTENTS
(Continued)

Chapter	Page
B.2 LabVIEW™ Control and Data Acquisition.....	58
B.3 Dose Control.....	66
REFERENCES.....	69

LIST OF TABLES

Table		Page
2.1	Dimensions and Operating Conditions of Source Electrodes.....	9
A.1	Properties of Decaborane.....	53

LIST OF FIGURES

Figure		Page
2.1	Schematic of the Beamline.....	6
2.2	Schematic of the Ion Source.....	7
2.3	Simulation of Ion Beam Extraction and Focussing.....	11
2.4	The Ion Source.....	12
2.5	Principle of Operation of Mass Analyzing Magnet.....	14
2.6	Sample Manipulator.....	17
2.7	Simulation of Deflection of Ion Beam.....	19
2.8	Vacuum and Gas Handling System.....	20
2.9	Gas Handling System.....	23
2.10	Structure of the Beamline.....	24
3.1	Ion Beam Spectrum for Argon at 9 keV in terms of Magnetic Field.....	26
3.2	Magnet Calibration Curve obtained from Fig. 3.1.....	28
3.3	Ion Mass Spectrum for Argon in terms of AMU obtained by converting Spectrum in Fig. 3.1 using Calibration Curve in Fig. 3.2.....	29
3.4	Micrometer Scanned Profile of Ar ⁺ Ion Beam in the Horizontal Direction.....	31
3.5	Magnet Scanned Profile of Ar ⁺ Ion Beam.....	31
3.6	Micrometer Scanned Profile of Ar ⁺ Ion Beam at 9 keV in the Vertical Direction.....	34
4.1	Mass Spectrum of Decaborane.....	36
4.2	Mass Spectrum of Decaborane on Wire Probe at 6 keV.....	37
4.3	Mass Spectrum of Decaborane on Sample Block at 6 keV.....	39

**LIST OF FIGURES
(Continued)**

Figure	Page
4.4 Scan of B ₁₀ Ion Beam along Horizontal Axis Perpendicular to the Beam.....	40
4.5 Fraction of Total B ₁₀ Current vs. Aperture Width.....	41
4.6 Implantation Experiment with Deflection.....	42
4.7 P- α Experimental Setup.....	44
4.8 Variation of Boron Dose on the Sample.....	44
4.9 Variation of Beam Current vs. Aperture Voltage.....	47
A.1 Structure of Decaborane Molecule.....	52
B.1 Control Circuit for Magnet Power Supply.....	57
B.2 Block Diagram of Magnet Control and Data Acquisition.....	59
B.3 Flowchart for Data Acquisition and Control.....	61
B.4 Front Panel of LabVIEW™ Program for Ion Spectrum.....	62
B.5 Functional Block Diagram-DAQ Analog Output (AO Update Channel).....	63
B.6 Functional Block Diagram-Wait Function.....	64
B.7 Functional Block Diagram-DAQ Read (Measure Pulse Width) and GPIB Read.....	66

CHAPTER 1

INTRODUCTION

The revolutionary growth of the semiconductor IC industry over the last three decades has been fueled by the aggressive reduction of transistor dimensions to fabricate IC chips with higher packing densities, greater circuit speeds and lower power dissipation. These advances led to the development of high-speed computers and complex processing systems with superior performance and drastically reduced cost per function today. This trend is expected to continue beyond the year 2000 when 0.1-micron technology will be in production [1]. Thus, the key challenge for the present day technology is the development of fabrication systems that meet this requirement [2].

Implantation of energetic ions into solids has played a critical role in the semiconductor industry over the last 25 years. It has been the primary technology for the doping of semiconductor layers in various parts of electronic devices, as well as fine adjustment of threshold voltage of MOS transistors. The advantages of Ion Implantation include the purity of the implanted species achieved by magnetic mass separation, precise dose control of the implanted species by ion current measurement and control of implantation depth by choice of ion energy. Advances in the CMOS fabrication technology have led to the production of 180 nm devices and presently, the development of 120 nm devices. As the quest for higher circuit density and smaller device dimensions continue, not only lateral but also vertical dimensions of the implanted layers become critical. Future generations of 0.1 μm devices will need junctions shallower than 50 nm.

Today's most challenging doping application is the formation of such ultra shallow junctions [3]. Although less of a problem for n-channel transistors where n-type source and drains are doped with heavy atoms of phosphorous or arsenic, it is a potentially major problem for p-channel transistors where the source and drain are doped with boron. Since B^+ atoms are light, their projected range in Silicon is much larger and therefore, they must be accelerated to very low energies of the order of 100 eV for ultra shallow implantation. However, generation and transport of ion beams of such low energy is hindered by the Coulomb forces to the point where attainable ion current becomes so small as to be impractical for commercial semiconductor implantation [4]. New schemes such as deceleration of energetic beams in front of the target and plasma immersion techniques are being investigated to solve this problem. Although implanters based on the deceleration technique have become recently available, their usefulness in addressing this problem is still in question [4]. Plasma immersion techniques do not discriminate among various ion species [5] and their potential for precise semiconductor doping remains uncertain. An alternative technique currently being developed is cluster or molecular implantation [6].

A cluster of n atoms impacting on a surface with kinetic energy E can be viewed as an impact of n atoms with energy E / n . Thus, we have the advantage of less energy per constituent atom in the case of cluster or molecular implantation. The other advantage of molecular implantation is the high charge to mass ratio with which an n atom cluster transports n times the mass of a monomer beam at the same current. Also, space charge problems (Coulomb repulsion) in the beam as well as problems of target charging are

minimized. The above features make molecular ion implantation an attractive alternative for shallow junction formation. [4]

Presently, BF_2^+ , which is heavier than the elemental B^+ ion, is used for shallow boron implantation. This allows a higher energy to be used for the same implant depth. Fluorine, however, is corrosive and can create voids in silicon, attack gate oxides and metal and enhance diffusion in gates. It is a problem particularly in thin oxides and small devices [3]. Recently, a new substance called decaborane has aroused great interest in the implantation community for possible use as an implant specie. It has been recently demonstrated at the Kyoto University, Japan that MOS devices with ultra shallow junctions have been formed using molecular ions of decaborane [8,9]. A molecule of decaborane consists of 10 boron atoms and 14 hydrogen atoms. Therefore, each boron atom in the molecular ion beam carries approximately $1/11^{\text{th}}$ of the beam energy and the boron dose per unit charge is 10 times larger than in the case of a monomer ion beam of boron. However, decaborane could not be used in conventional ion implanters successfully because the $\text{B}_{10}\text{H}_{14}$ molecule is destroyed in the plasma generated by most ion sources. Thus, a study had to be carried out to learn more about the ionization properties of decaborane and an ion source had to be designed that could generate an ion beam of decaborane.

This thesis contains information pertaining to the work carried out at the Ion Beam and Thin Film Research Laboratory at NJIT on the design and construction of a research ion implanter for investigating the properties of the generated decaborane ion beam and also for implantation of decaborane in Si.

The main objectives of the research were:

- 1) To study the feasibility of generating ion beams of decaborane
- 2) To design and construct a decaborane ion source for low energy implantation (upto 20 keV).
- 3) To design and build a research ion implanter for implanting decaborane.

In the next phase of this research program, the characteristics of Si implanted with decaborane ions will be investigated.

A recent MS thesis was dedicated to the design and construction of the ion source [10]. The thesis presented here concentrates on the design and construction of the experimental beamline with a mass separation magnet. It describes the work on the implanter electrical system, magnetic mass separation and ion beam diagnostics. It includes the design of data acquisition system and control based on a PC running LabVIEW™ software.

Chapter 2 deals with the design and construction of the beamline and describes the individual components of the beamline namely the ion source section, the magnet section and the sample chamber with deflection plates. This chapter also describes the vacuum and gas handling system. Testing of the implanter using argon ions, including calibration of the magnet with Ar^+ and Ar^{++} ions, and beam profiling are discussed in Chapter 3. Chapter 4 deals with experiments carried out to obtain the mass spectrum of decaborane, beam profile of the B_{10} ion beam, and implantation and deflection experiments. Summary and Conclusions during the course of this thesis are discussed in Chapter 5. Appendix-A contains information on the physical and chemical properties of

decaborane and safety measures to be taken when handling it. Appendix-B describes electrical systems for magnet control, ion current and dose measurements, and the data acquisition system using LabVIEW™ software.

CHAPTER 2

EXPERIMENTAL ION IMPLANTATION SYSTEM

The experimental ion implantation system was designed and built for investigating the properties of the decaborane ion beam and also for implantation of decaborane in Si. The ion beam generated in the source was mass analyzed for selecting the ion species of interest for implanting into the target. The research ion implantation system is schematically represented in Fig. 2.1. The length of the beam path from the source to the sample chamber is approximately 2 meters (7 feet).

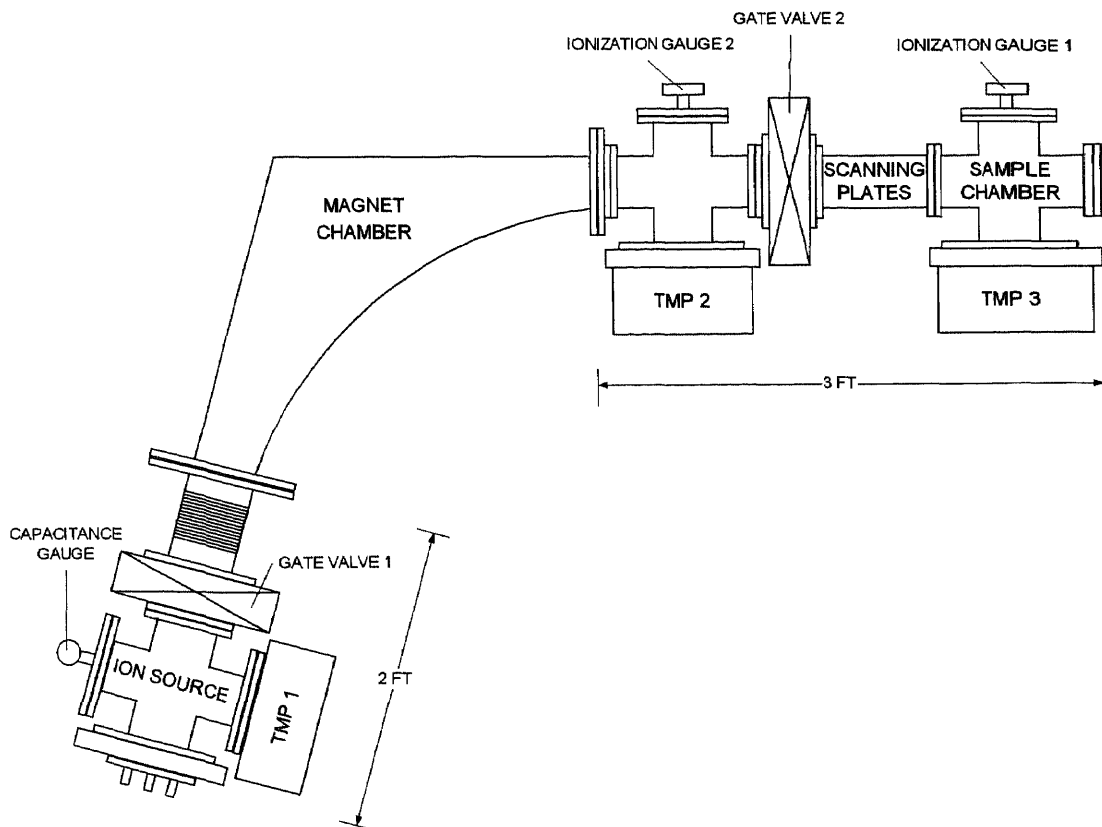


Fig. 2.1 Schematic of the Beamline

The beamline consists of the following main sections.

- Ion source and source chamber
- Mass analyzing magnet and magnet chamber
- Sample chamber with deflection plates

The three sections are pumped by separate high-vacuum pumps and are separated by gate valves. The details of the vacuum system are described in Section 2.4.

2.1 Ion Source

The design of the ion source is based on the Bayard-Alpert ionization gauge, which was converted into a usable ion source by appropriate modification of the electrode structure and applied voltages [11,12,13]. The ion source was designed and built by Ravidath Gurudath during the work on his MS thesis [10].

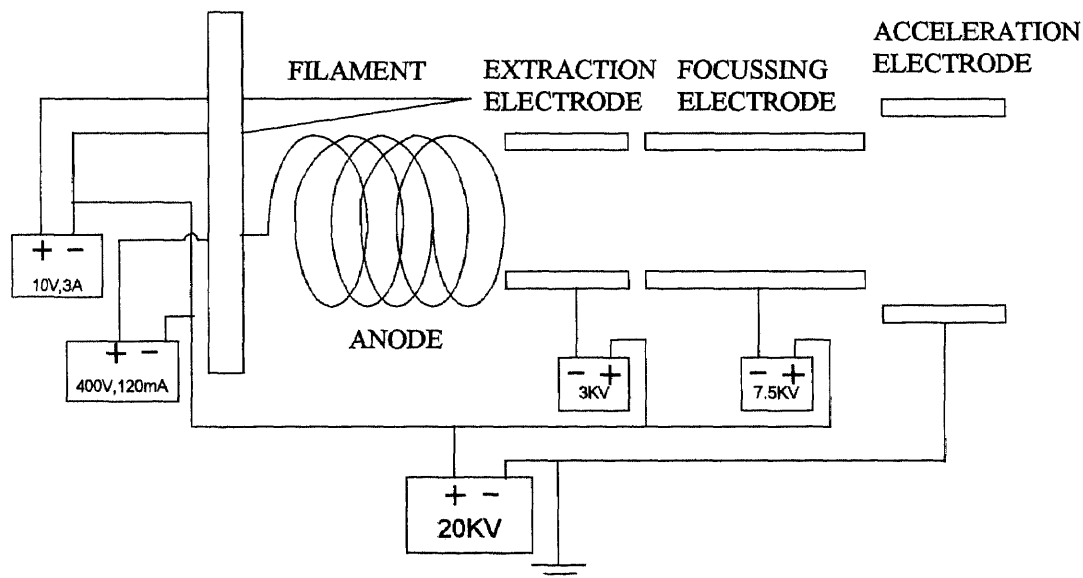


Fig. 2.2 Schematic of the Ion Source

2.1.1 Construction and Operation

The schematic of the ion source with the electrical connections is shown in Fig. 2.2. The ionizer section of the ion source consists of the cathode and the anode. The cathode is a tungsten filament (0.005" dia), which is heated by a current of a few amperes and the anode is made up of a helically wound tungsten wire (0.015" dia), which collects the electrons emitted by the cathode. The inlet gas is ionized in the region between the cathode and the anode by interaction of energetic electrons with the gas molecules. This is known as electron impact ionization and was used as the means of ionizing decaborane vapor since it provides the control of electron energy, which determines the ionization and dissociation rates. The ionizer design allows for multiple passes of electrons through the ionizer volume before they are collected by the anode, thus increasing the ionization efficiency. Ions created in the ionizer are extracted and focussed to form an ion beam by the ion extraction system, which consists of the extraction electrode, the focussing electrode and the ground electrode. The extraction electrode attracts the positively charged ions when a potential difference is applied between the ionization chamber and the extraction electrode such that the ionizer is at a higher potential than the extraction electrode. The focussing electrode, which follows the extraction electrode, is more negative than the extraction electrode and it helps in shaping the beam and focussing the beam at a desired distance. The 20 kV high-voltage power supply is used to set the energy of the ion beam. The power supplies for the extraction and focussing electrodes are isolated from ground by an isolation transformer and are connected to the electrodes in the source by feed-throughs isolated by ceramic insulators. The cylindrical electrodes

were machined from stainless steel while the electrode support assembly was constructed from eV parts supplied from Kimball Physics [14].

Table 2.1 Dimensions and Operating Conditions of Source Electrodes

Electrode	Dimensions	Typical Operating Voltage
Filament	Tungsten wire of 0.005" dia	10 V*
Anode	Tungsten wire of 0.015" dia (spirally wound for 5 turns)	80 V
Extraction	Stainless steel tube 20mm long held by C series eV plate with 0.5" hole at the center	-200 V
Focussing	40 mm long Stainless steel tube held by C series eV plate with 0.5" hole at the center	-1500 V
Acceleration	20 mm long Stainless steel tube held by C series eV plate with 0.75" hole at the center	0 V

* One end of the filament was at 0 V and the other was at 10 V for a heating current of 2.3 A.

2.1.2 Simulation of the Ion Source

The operation of the ion-source was simulated using an ion optics program called SIMION [15], which is a PC based ion optics simulation program that models ion optics problems with 2D symmetrical or 3D asymmetrical electrostatic or magnetic potentials. It incorporates a so called "*ion optics workbench*" that allows sizing, orientation and positioning of up to 200 instances (2D or 3D images) of "*potential arrays*" within the workbench space that define the geometry and potentials of the electrodes and magnetic poles. The potentials of points outside electrodes and poles are determined by solving the Laplace equation by finite difference methods. Ions can be flown within the workbench volume and their trajectories are determined by the fields of the potential array instances they fly through. Ions can be flown in singly or in groups, displayed as lines or dots, and automatically be "*re-flown*" to create movie effects. Other features include data recording, charge repulsion, user programs and geometry files. The program does not account directly for the space charge of the ions. It is assumed that in the simulation of ion trajectories, the space charge density of the extracted beam is low and can be neglected. The space charge effect, however, may be important in the distribution of electrons and ions in the ionizer volume.

Fig. 2.3 shows the simulation for one set of extraction and focussing conditions. The blue lines represent the trajectory of the beam and the red lines represent the equipotential surfaces. The simulations provided information about the ion beam trajectory for various extraction and focussing conditions and helped to establish voltages on the extraction and focussing electrodes.

The source flange is mounted on a 20 kV High voltage bushing*, which isolates it from the rest of the beamline. This allows operating the source at high voltage while the rest of the beamline, including the target chamber is at ground potential. A circular aperture of 0.25" dia, which is mounted in front of the source at a distance of 8.5" from the source flange, defines the entrance of the ion beam to the magnet chamber.

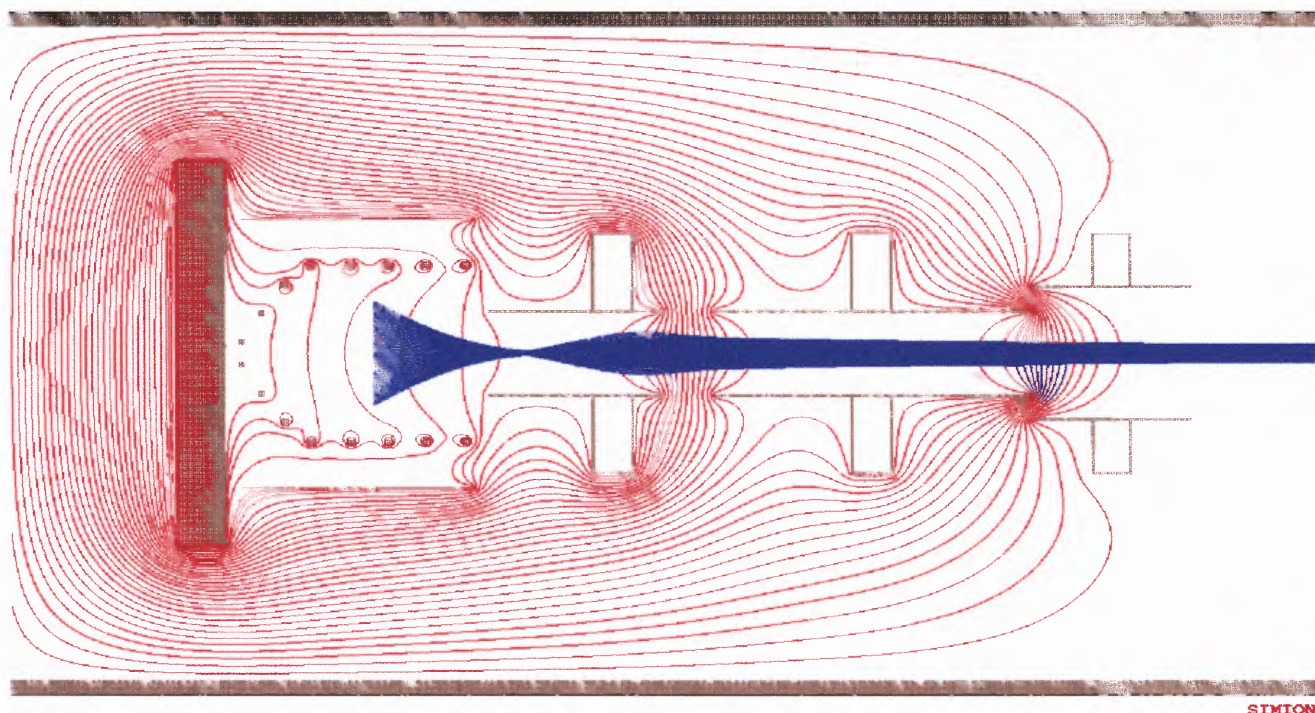


Fig. 2.3 Simulation of Ion Beam Extraction and Focussing

* The high voltage bushing is a part from an ion implanter from Eaton Corporation, which makes possible mounting of the source on Eaton NV-3204 ion implanter.

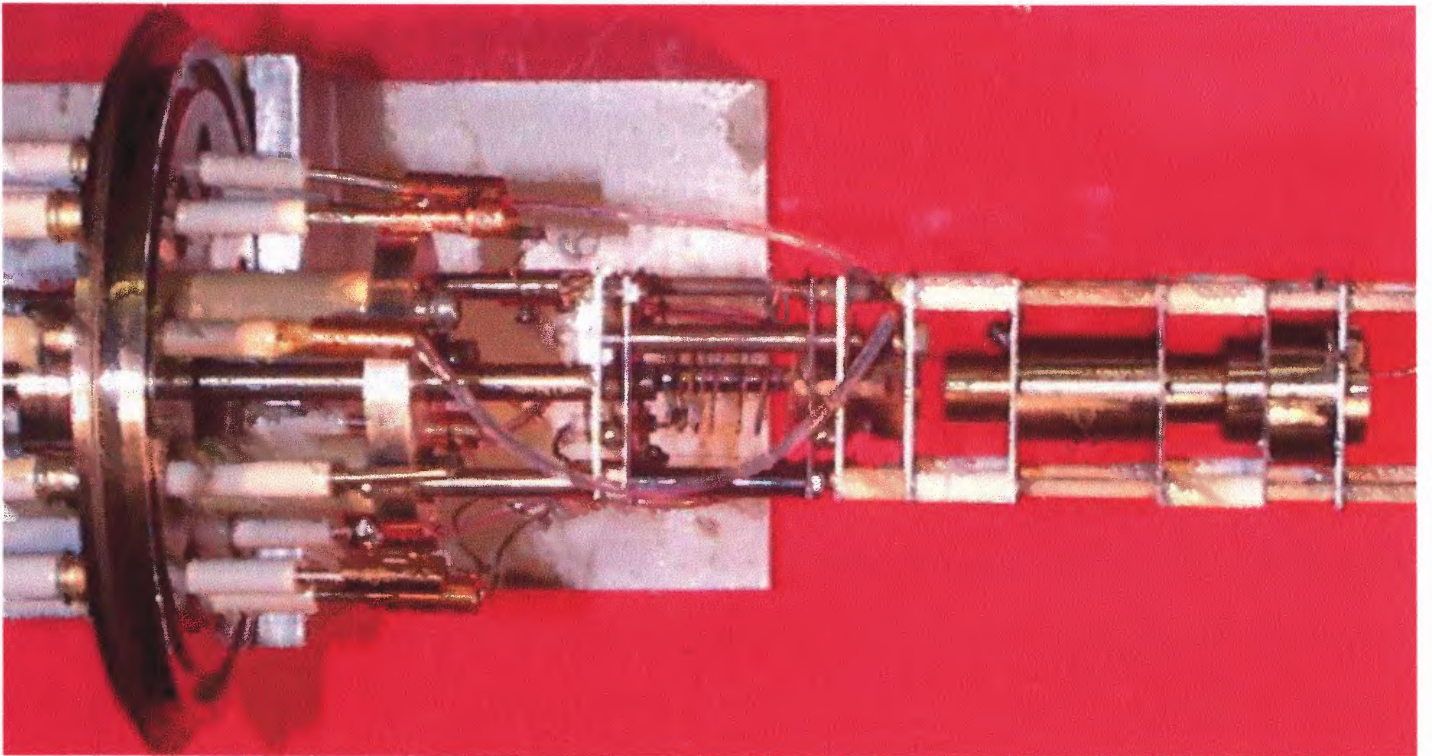


Fig. 2.4 The Ion Source

2.1.3 Notes on the Operation of the Ion Source

During operation of the ion source several problems were encountered and solved or described below:

- Magnitude of ion current observed was of the order of nanoamperes due to misalignment of the source with respect to the axis of the beamline. By moving the source chamber with respect to the magnet in the vertical direction, the beam current at the sample chamber was maximized.
- Operation of the ion source was restricted to energies lesser than 9 keV because of excessive arcing and plasma discharge. This was improved by turning inwards the sharp edges of the screws connecting the feedthroughs to the electrodes inside the source.
- Steady decrease in electron current was observed as the high voltage to the source was increased. This was because the electrons were escaping through the anode spiral to the ground. Enclosing the ionizer structure by a thin stainless steel strip solved this problem.
- Burning out of quad op-amp chips used in the control circuit for the magnet power supply occurred due to transients generated by a sudden discharge of the high-voltage power supply. Addition of resistors ($22\text{ M}\Omega$, 0.5 W) in series with extraction electrode, focussing electrodes and ground electrode reduced the occurrence of this problem.

2.2 Mass Analyzing Magnet

The mass analyzing magnet, which is positioned in between the source and target chamber, lets us choose the particular ion specie with specific mass for implantation into the target. A current flowing through the magnet windings creates a magnetic field with vertical field lines perpendicular to the path of the ion beam.

2.2.1 Principle of Operation

The principle of operation of the magnet is schematically given in Fig. 2.5. As the ions move through the magnetic field, they are forced to move in a circular path with according to Fleming's left-hand rule. The radius of curvature of the ion beam can be changed by changing the current flowing through the magnet windings. The outer wall of the magnet chamber stops heavier ions while the inner wall stops the lighter ions. Only ions with specific mass to charge ratio are allowed to pass through the center of the magnet.

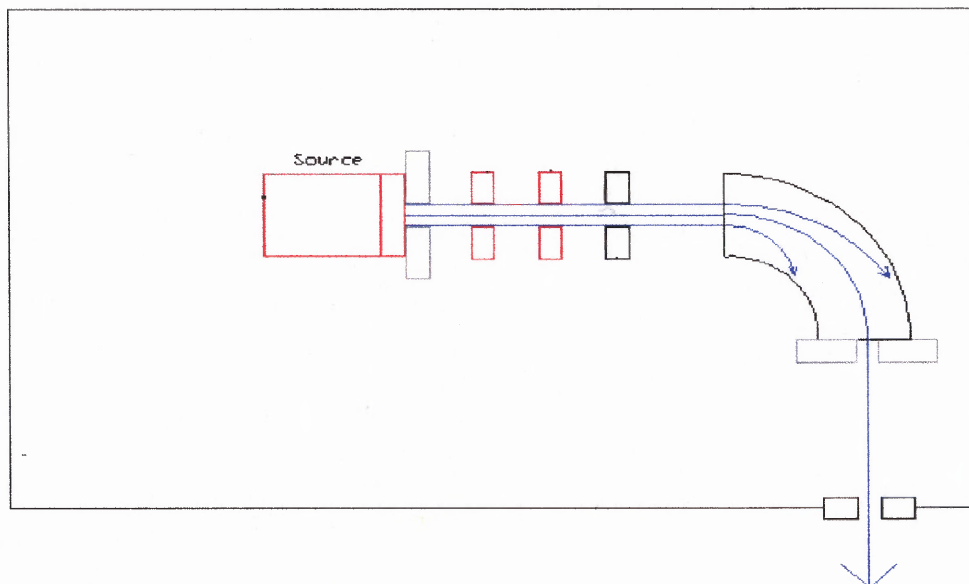


Fig. 2.5 Principle of Operation of Mass Analyzing Magnet

The radius of curvature of the ions through the magnetic field is given by [16]

$$r = \frac{1}{B} \sqrt{\frac{2mV_{ext}}{q}} \quad (2.1)$$

Where : r is the radius of curvature of the ions in meter

B is the magnetic field in tesla

V_{ext} is the potential through which ions are accelerated in volts

q is the charge on the ion in coulomb

m is the mass of the ion in kg

The pole pieces of the magnet shaped in such a way that the magnetic field continuously increases in intensity for an ion trajectory of increasing radius and continuously decreases in intensity for an ion trajectory of decreasing radius. An ion beam of a single mass, which is focussed in front of the magnet at a point called object distance, enters the magnet with different trajectories. Each of these ion beams with different trajectories comes under the influence of a different magnetic field and the net effect is that each of the ion beams is brought to focus at a point after the magnet called the image distance. This focussing occurs only in the horizontal plane and not in the vertical plane, since the magnetic field is not a function of distance traveled by the ion in the magnet.

2.2.2 Specifications

The magnet used in the ion implantation system is a 70° sector magnet from a NV-10 ion implanter from Eaton Corporation and the radius of the main trajectory of an ion beam is

21.18". The object distance for the magnet is 10.5", which is the distance between the point where the ions are brought to focus by the ion source and the entrance to the magnet. The image distance for the magnet is 14.5", which is the distance between the beam exit point of the magnet and the point after the magnet where the ions are focussed. According to nominal specifications, the magnet is rated at 8.5 kgauss for a current of 150 A. A freewheeling diode connected in parallel across the coils provides a path for the current to flow when input current to the magnet is suddenly shut off. The magnet windings are cooled by water.

2.3 Sample Chamber and Deflection Plates

This section of the experimental implanter contains apertures for defining the beam size, deflection plates for scanning and controlling the beam position and a sample holder for implantation experiments.

2.3.1 Sample Chamber

The sample chamber is made from a 6-way DependexTM cross and is mounted at the end of the beamline after the deflection plates. A sample manipulator with sample block, as shown in Fig. 2.6, is mounted on the upper port of the cross. The samples to be implanted are mounted on a 2.25" × 1.2" sample block made of Aluminum. This block is a part of a sample manipulator, which can be moved by micrometer screws in the x, y and z directions by 0.5" and also has the capability to rotate 360° around its vertical y-axis*. The block can also be moved along the y-axis in four steps with a distance of 0.4"

* Here x is defined as a horizontal axis and y as a vertical axis, both perpendicular to the beam. z-axis is along the beam.

between steps. This allows mounting multiple samples on different sides of the sample block and switching between different samples by rotating the sample manipulator and by adjusting its vertical position. Current measurements were taken from a wire of 0.065" dia, which is mounted 0.2" in front of the sample block. Another wire, which is offset from the center by 1.2", is used in deflection experiments and rotary beam profiling, which are explained in subsequent chapters.

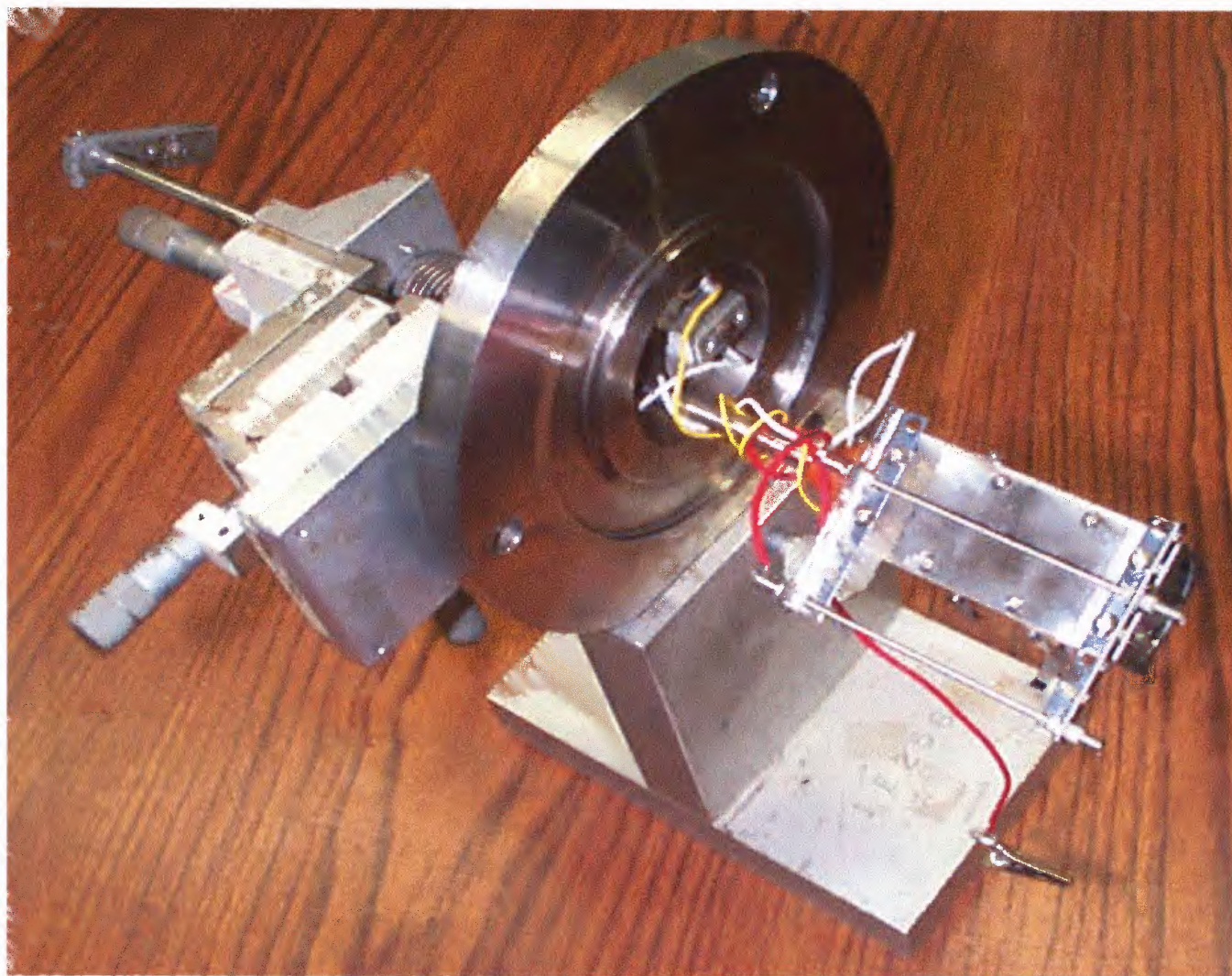


Fig. 2.6 Sample Manipulator

2.3.2 Deflection Plates

The deflection plates are used to deflect and scan the beam across the sample for uniform implant dose across the wafer. The dimensions of the deflection plates that are length 5.8", width 2", thickness 0.2" and the distance between plates is 1.5".

The total distance by which the beam can be deflected on a sample is given by the equation:

$$s = \frac{xV_d(l + \frac{x}{2})}{2dV_a} \quad (2.2)$$

Where : s is the total deflection of the beam on the sample

x is the length of the deflection plates

V_d is the deflection voltage in volts

l is the distance of the sample from the end of the deflection plates

d is the distance between the deflection plates

V_a is the beam acceleration voltage in volts

Fig. 2.7 shows the simulation of the deflection of an ion beam due to the field between the deflection plates when a positive voltage is applied to the bottom plate while the top plate is at ground potential. The simulation with SIMION shows that the beam experiences negligible focussing effect due to deflection voltage and thus can be used for deflection and scanning purposes. The simulation also established the voltage necessary for deflection on the sample.

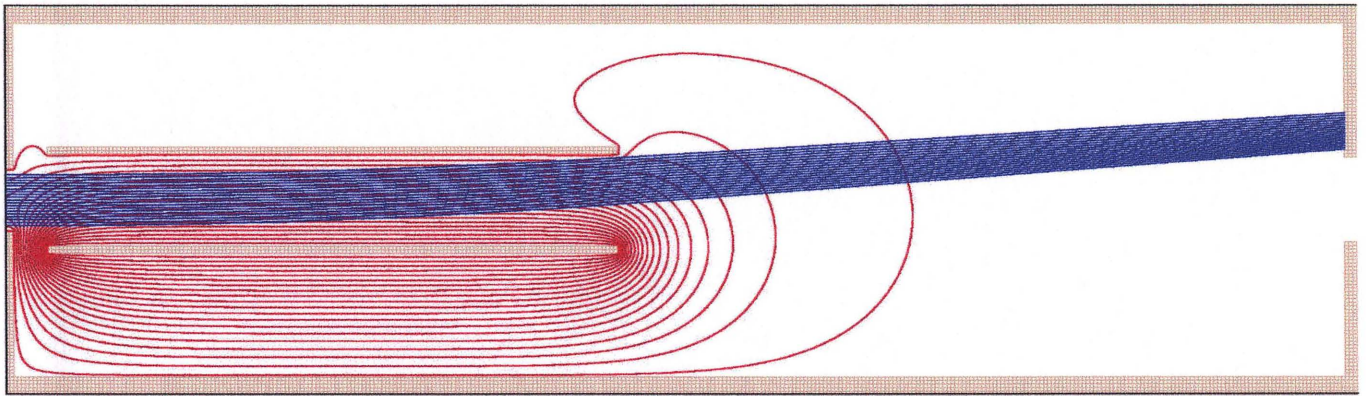


Fig. 2.7 Simulation of Deflection of Ion Beam

2.4 Description of Beamline, Vacuum and Gas Handling System

The beamline of the research ion implantation system is designed and built using 4" Dependex™ type vacuum parts. Transition flanges to Conflat from Dependex™ were machined for connecting turbo pumps and gate valves to Dependex™ crosses. The vacuum and the gas handling system for the ion implanter were designed by taking into consideration the following factors.

- 1) Toxic nature of decaborane. [Ref Appendix-A]
- 2) Ease of switching between decaborane and argon gas inlets.
- 3) Independent venting of individual sections of the beamline.

The schematic of the vacuum and gas handling system is shown in Fig. 2.8.

2.4.1 Beamline Section

A 4-way, 4" Dependex™ cross serves as the source chamber and is connected to the magnet chamber through a gate valve and bellows. The gate valve provides the option of shutting off the ion source chamber from the rest of the beamline.

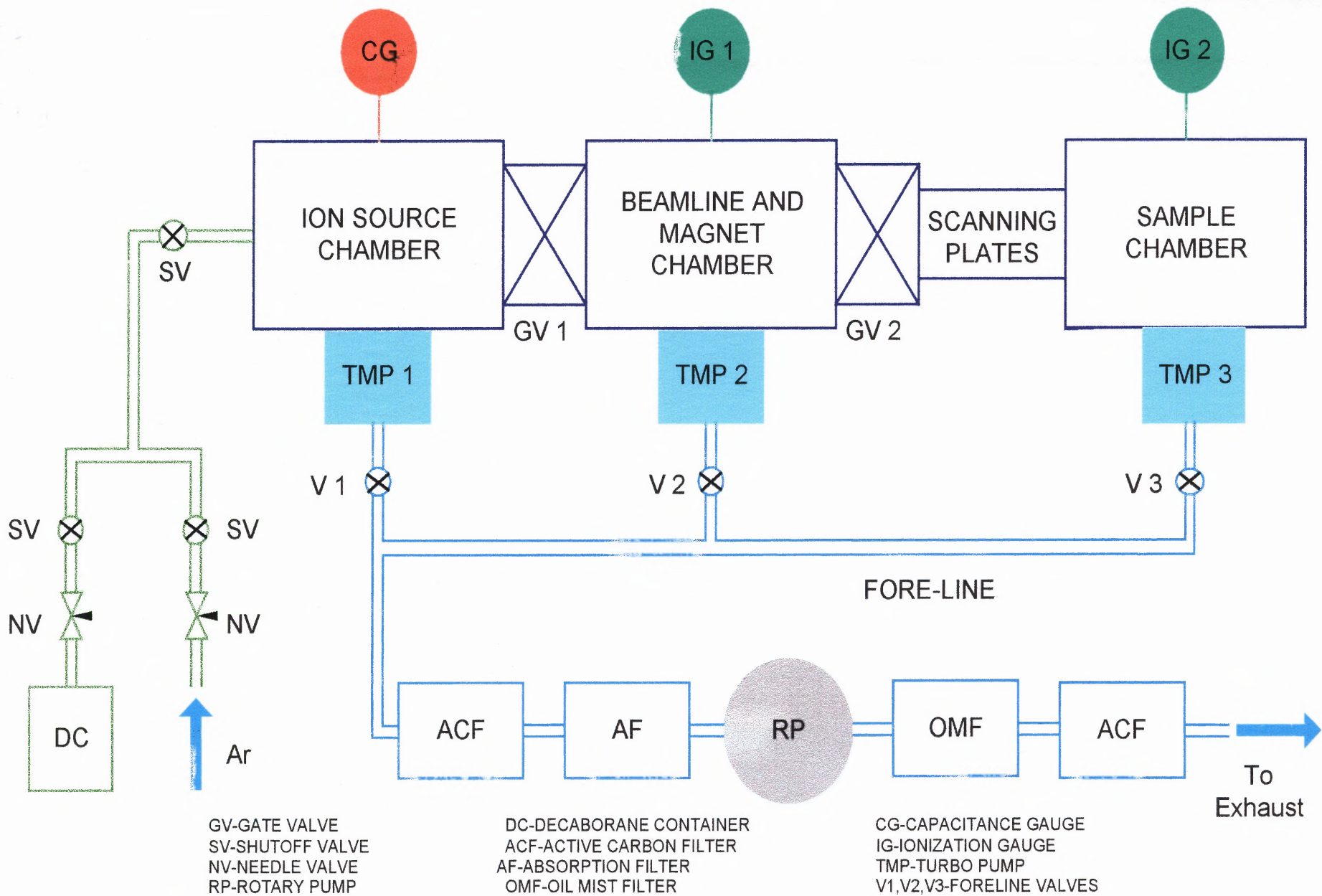


Fig 2.8 Vacuum and Gas Handling System

The bellows, and the adjustable mounting fixture, allow us to change the position of the source to adjust the direction of entry of the ion beam in the magnet chamber. The source is pumped by a Pfeiffer Balzers turbo-molecular pump (pumping speed 170 l/s), that is attached to the lower port of the source chamber. Attached to the upper port of the cross is a 627B Baratron pressure gauge from MKS Instruments operating in the range 1×10^{-5} to 0.02 torr, which is used to measure the pressure in the source. The magnet chamber is pumped by a water-cooled Leybold-Heraeus turbo-molecular pump (pumping speed 360 l/s), which is attached to one of the side ports of a 4-way Dependex™ cross, which in turn is attached to the magnet chamber. Attached to the opposite port of the 4-way cross is an ionization gauge, which is used to measure the pressure in the magnet chamber. The deflection plates and the sample chamber are connected to the magnet through a gate valve, which helps us to quickly change the implant samples by venting only the sample chamber and leaving the rest of the beamline under vacuum. A 4", 6-way Dependex™ cross serves as the sample chamber. The sample holder is mounted on the top port of the 6-way cross. A Leybold-Heraeus turbo-molecular pump (pumping speed 150 l/s), which is attached to one of the side ports of the 6-way cross, pumps the sample chamber. An ionization gauge attached to the bottom port of the cross reads the pressure in the sample chamber.

The sections of the beamline are vented with pure nitrogen. The typical base pressures obtained for the individual sections are 1.5×10^{-7} torr in the source chamber, 3.0×10^{-6} torr in the magnet chamber and 2×10^{-6} torr in the sample chamber.

2.4.2 Vacuum Foreline and Filter Section

Each of the individual sections of the beamline is connected to a common foreline, which is pumped by a single rotary pump. The foreline is connected to the different sections of the beamline by foreline valves V1, V2, V3 as shown in Fig. 2.8. By this method of connection, the individual sections of the beamline could be vented and pumped easily by closing and opening the foreline valves in conjunction with the gate valves. Also, possible decaborane contamination could thus be restricted to a single rotary pump. A number of filters are connected in series with the rotary pump. An absorption filter (AF), connected to the pumping port of the rotary pump, absorbs any back-streaming oil from the pump. An active carbon filter, connected between the AF and the foreline, absorbs any toxic decaborane vapor as it is being pumped out of the system. Connected to the exhaust port of the rotary pump is an oil mist filter followed by a second active carbon filter as a precaution against any toxic vapor that may pass through the rest of the pumping system. The output from the last filter is connected to the exhaust fan and diluted in air leaving the laboratory.

2.4.3 Gas Handling System

The gas manifold system shown in Fig. 2.9 was designed and built using VCRTM and SwagelokTM type gas fittings. The gas inlet to the source is separated into the inlet for decaborane vapor and the inlet for argon, which is used to calibrate the magnet. There are separate shut-off valves and needle valves controlling gas flow on both argon and decaborane lines. There is also a main shut-off valve on the line leading to the source.

Decaborane powder is contained in a glass tube of 0.25" O.D. and 1.5" height, and is transported to the ion source by sublimation.

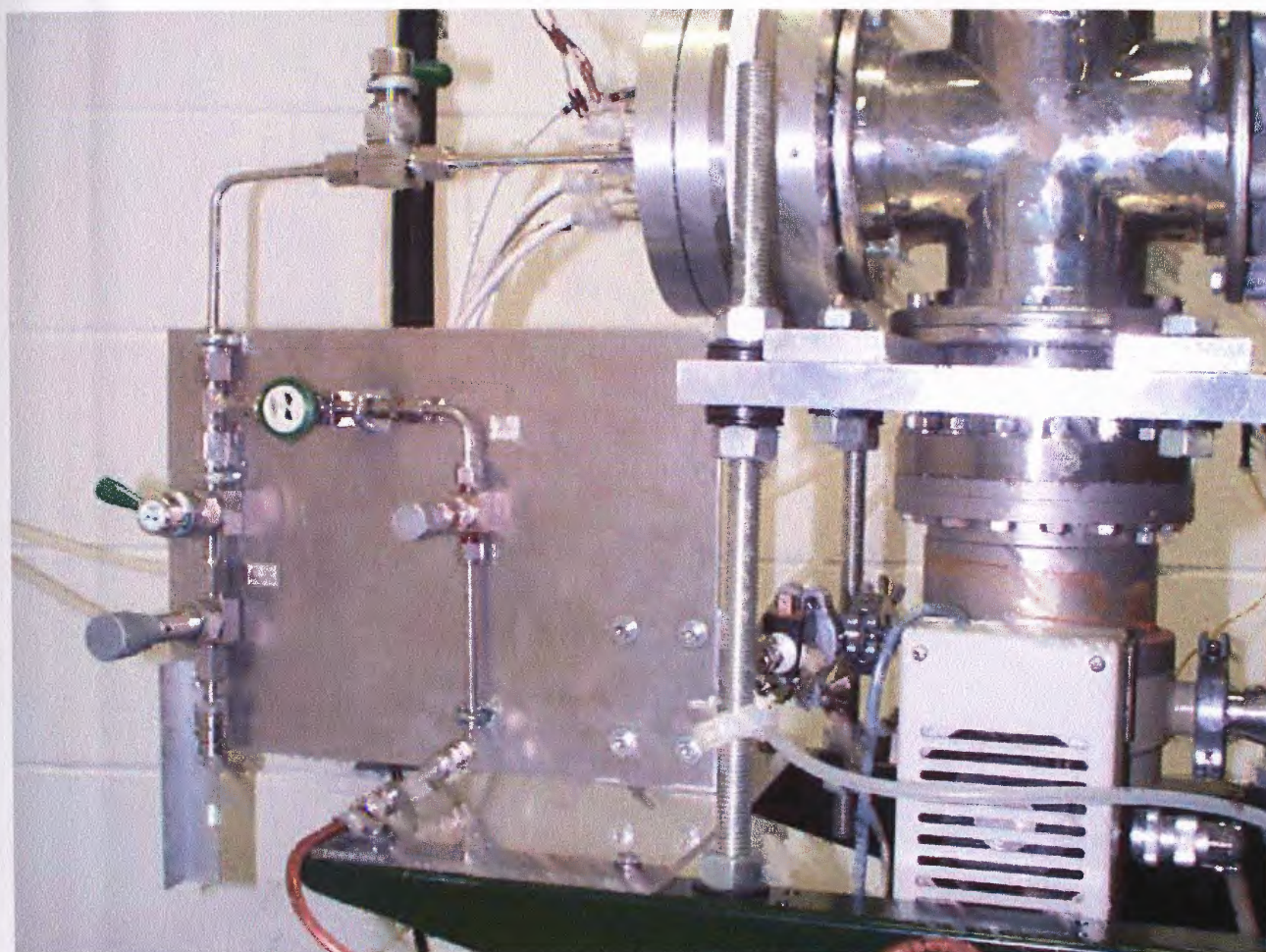


Fig. 2.9 Gas Handling System

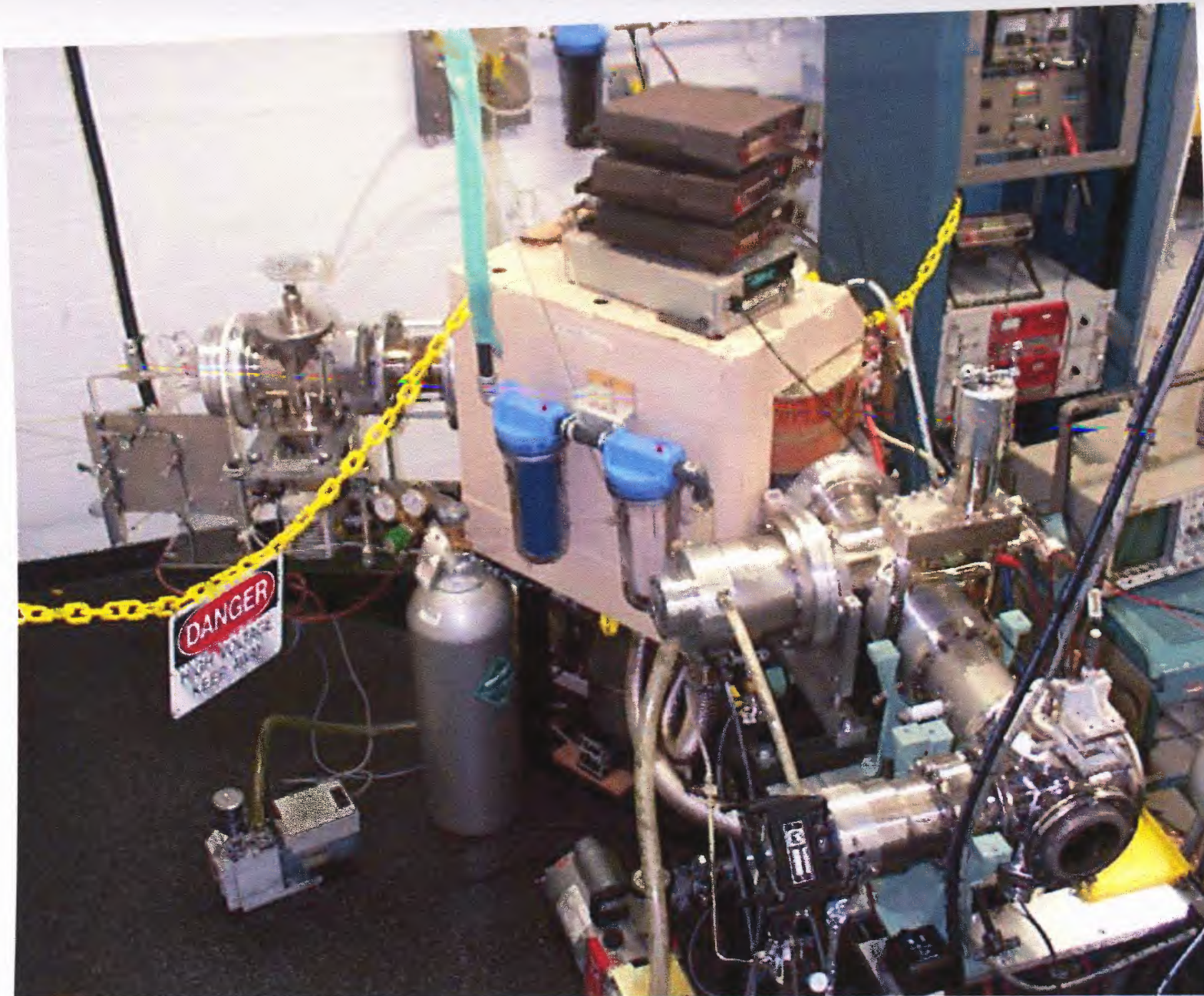


Fig. 2.10 Structure of the Beamline

CHAPTER 3

EXPERIMENTS WITH ARGON AND MAGNET CALIBRATION

The general operation of the implantation system that was described in Chapter 2 was first tested and analyzed by using argon ions. Argon has advantages as a test gas because it is monatomic and inert in nature. It is also suitable for calibration of the magnet because its natural form consists practically of a single isotope ^{40}Ar ($^{40}\text{Ar} = 99.600\%$, $^{38}\text{Ar} = 0.063\%$ and $^{35}\text{Ar} = 0.337\%$).

By using argon, with Ar^+ and Ar^{++} ion species, a spectrum of ion current vs. magnet current was measured from which a calibration curve for the magnet is plotted in terms of ion current vs. ion mass in Atomic Mass Unit (AMU). Also, a study of the size and shape of the Ar^+ ion beam after mass analysis was carried out to determine the width of the aperture required to allow ions of given masses to enter the sample chamber.

Argon was let into the source through a needle valve, which controlled the flow of gas. For these experiments, typical operation conditions for the source were filament current 2.2 A and anode voltage 80 V. Electron current observed for filament and anode settings was ≈ 10 mA. For ion energy of 9 keV, typical extraction settings were extraction voltage of -490 V and focussing voltage of -2490 V. Typical source operating pressure measured by an ionization gauge was 1×10^{-5} torr. The rest of the beamline was at 2×10^{-6} torr. The control circuits for magnet power supply and measurements of ion current are given in Appendix-B.

3.1 Ion Mass Spectrum of Argon and Calibration of Mass Analyzing Magnet

In order to convert the spectrum of ion current with respect to the magnet current to an ion mass spectrum as a function of ion mass in terms of AMU, the magnet was calibrated by identifying peaks of known masses in the ion beam spectrum.

3.1.1 Ion Beam Spectrum

The spectrum for argon was obtained as shown in Fig. 3.1, by increasing the magnet current in uniform steps.

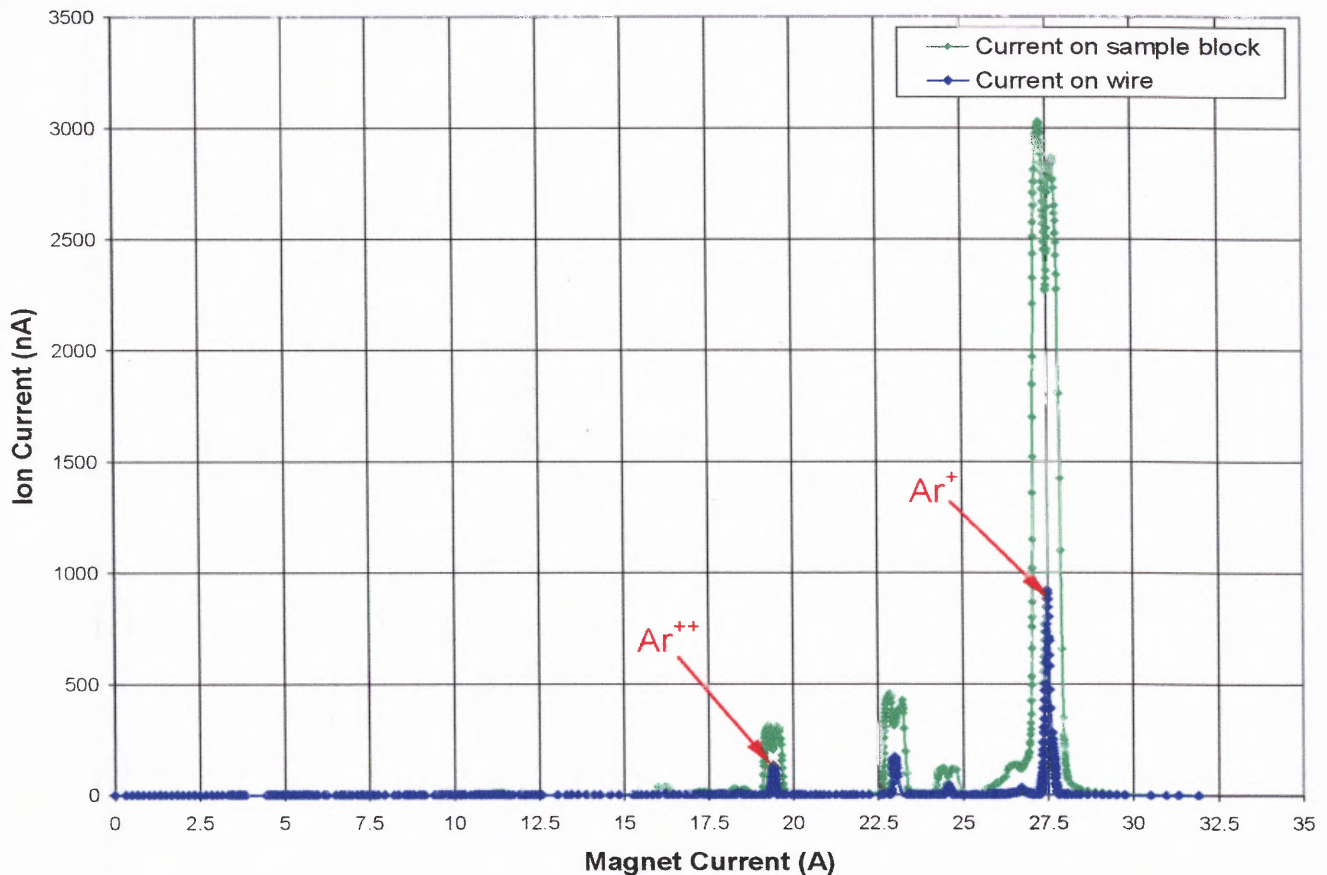


Fig. 3.1 Ion Beam Spectrum for Argon at 9 keV in terms of Magnetic Field

For each step, the ion current was measured on a wire probe of 0.06" dia and simultaneously on the sample block described in Section 2.3.1, and a graph of ion current

vs. magnet current was obtained. The entire process was computer controlled using Data Acquisition and GPIB interfaces and LabVIEW™ software. For a detailed description of Data Acquisition and LabVIEW™ control see Appendix-B. Although a current from the wire probe is taken for calibration purposes, since it provides good mass resolution, a comparison of current obtained on the block and the wire is shown in Fig. 3.1. It is seen that the magnitude of current obtained on the sample wire is $\sim 1/3$ of the current obtained on the block. The highest peak was identified as Ar^+ since it is the main component in the argon ion spectrum. Since Ar^{++} is doubly charged but has double the energy of the singly charged Ar^+ ion, the peak for Ar^{++} is observed at a magnet current that is $1/\sqrt{2}$ times the magnet current for which the Ar^+ peak is observed. Thus, the Ar^{++} peak has the same position in the spectrum as a singly charged ion with half the mass of Ar^+ .

3.1.2 Calibration Graph and Ion Mass Spectrum

On plotting a graph of the square root of ion mass in AMU for the two peaks of argon vs. magnet current, a calibration curve for the magnet has the form of a straight line as shown in Fig. 3.2. The equation of the calibration curve is used to convert an ion beam spectrum from the magnet current setting to AMU. The resulting ion mass spectrum for argon using the calibration curve is shown in Fig. 3.3. The accuracy of the calibration is confirmed by the fact that the curve misses the origin of the co-ordinate system by only 10^{-3} AMU. Other peaks in the graph were identified based on the mass, namely H_2O (18), CO (28), O_2 (32). The calibration curve obtained for a given energy can be used for obtaining a calibration curve for a different energy since the magnet current is proportional to square root of ion energy.

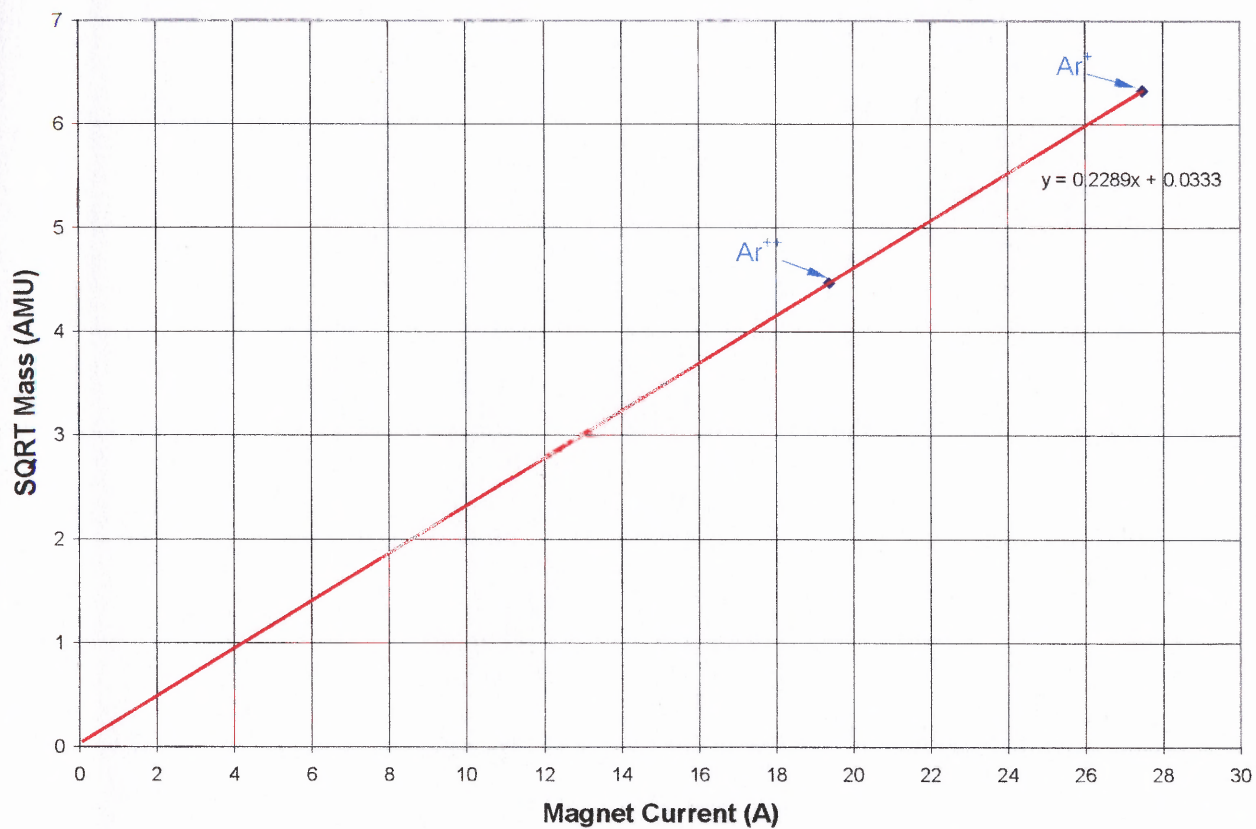


Fig. 3.2 Magnet Calibration Curve obtained from Fig. 3.1

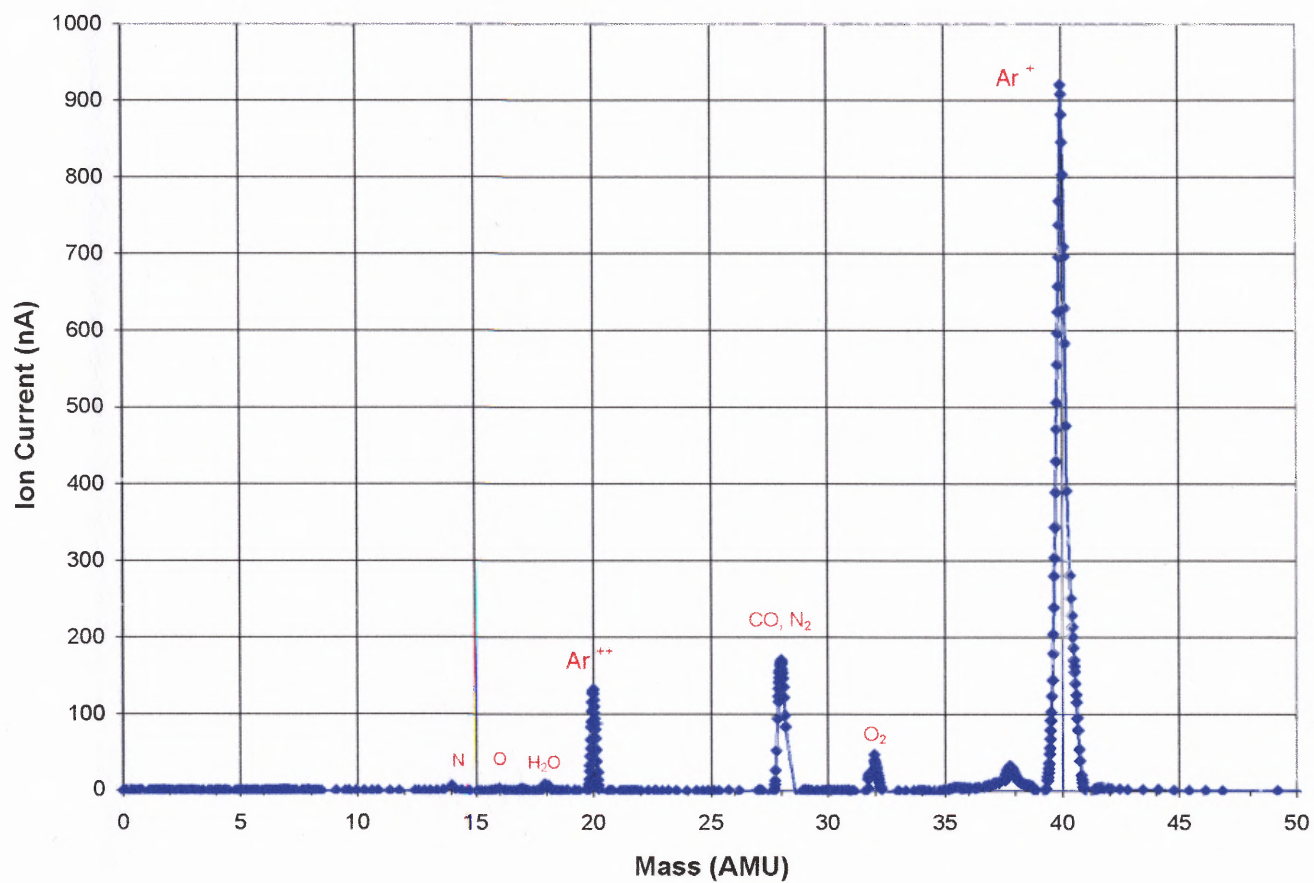


Fig. 3.3 Ion Mass Spectrum for Argon in terms of AMU obtained by converting Spectrum in Fig. 3.1 using Calibration Curve in Fig. 3.2

3.2 Argon Ion Beam Profiling in the Horizontal Plane

A study of the size and shape of the Ar^+ ion beam after mass analysis was carried out in order to determine the width of the aperture that would allow ions in a given mass range to enter the sample chamber. A horizontal micrometer scan was performed and compared with a profile obtained by variation of magnetic field.

3.2.1 Micrometer Beam Profiling in the Horizontal Plane

Profiling of the argon ion beam was done in the horizontal direction by traversing a metal strip of 0.2" in width and 2.25" in height across the ion beam in discrete steps by using micrometer screws. By measuring ion current on the metal strip for each point, a plot of ion beam current vs. micrometer position was obtained, as shown in Fig. 3.4. From the plot, we infer that the width of the beam is comparable to the width of the metal strip used, and is 0.3" at half maximum.

3.2.2 Beam Profiling by Magnetic Field Variation

The profile of the Ar^+ ion beam with respect to variation magnetic field was obtained by increasing the magnet current in discrete steps and by noting the ion current on a metal strip of 0.2" in width and 2.25" in height for each step. The resulting plot of ion current vs. magnet current, which is proportional to magnetic field, is shown in Fig. 3.5. A comparison of the widths of the ion beam obtained with the micrometer scan and the magnet scan was made to verify our understanding of the magnet operation.

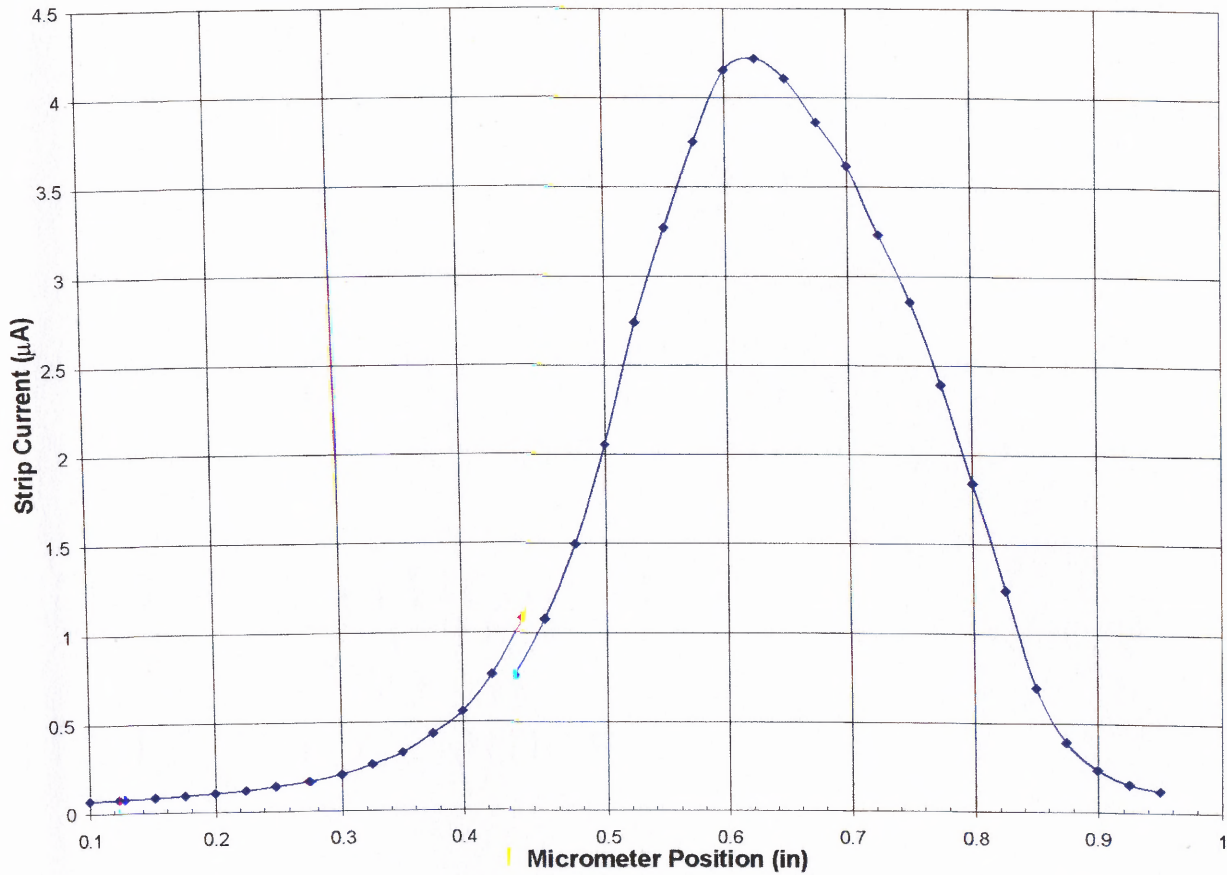


Fig. 3.4 Micrometer Scanned Profile of Ar^+ Ion Beam in the Horizontal Direction

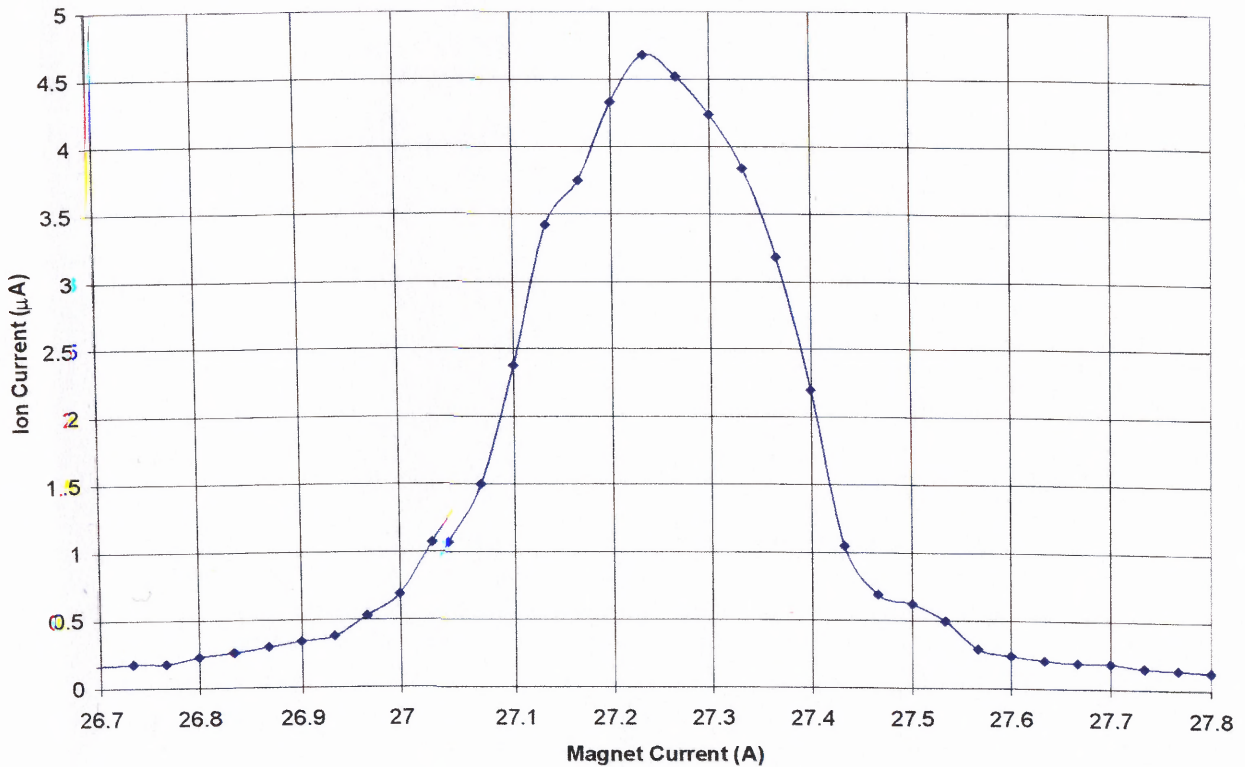


Fig. 3.5 Magnet Scanned Profile of Ar^+ Ion Beam

3.2.3. Comparison of Micrometer and Magnet Scans

One of the important specifications of the magnet is the ability of the magnet to separate an ion of mass m from an ion of mass $m + \Delta m$. Assuming that the field has been adjusted to allow an ion of single charge and mass m to follow a circle of radius r , an ion of mass $m + \Delta m$ will be displaced by a distance [17]

$$\Delta x = \frac{r}{2} \frac{\Delta m}{m} \left[1 - \cos \phi + \frac{L}{r} \sin \phi \right] \quad (3.1)$$

Where : r is the radius of the magnet

L is image distance of the magnet

m is the mass of the ion

ϕ is the angle of deflection of the ion beam by the magnet

Δm is the incremental change in the mass of the ion, which is displaced by

Δx from the ion of mass m at distance L from the magnet

The width of the beam at half maximum in terms of magnet current from Fig. 3.2 is (27.4 A - 27.1 A) = 0.3 A. The magnet current where the maximum ion current is obtained is 27.22 A. Thus, the ratio $\Delta I/I$ is 0.3 A / 27.22 A = 0.011. Since we know that ion mass m depends on the square of the magnetic field B (Eq. (2.1)), the ratio $\Delta m/m$ is equal to the ratio $2\Delta B/B$ where B is the magnetic field for mass m . Also, since the magnetic field is proportional to the magnet current, $\Delta B/B$ is equal to $\Delta I/I$. Thus,

substituting the value of $2\Delta I/I$ for $\Delta m/m$ in Eq. (3.1), the value of Δx is obtained as 0.3". This is in agreement with the half width of the beam obtained as 0.3" from Fig. 3.4.

These experiments also helped in establishing the thickness of the wire to be used for beam profiling to obtain better mass resolution. From Eq. (3.1), Δm is proportional to mass m for a given Δx . Therefore, the number of masses contained within Δx for a higher mass is more than the number of masses contained within Δx for a lower mass. Since the mass of decaborane, is 2.93 times that of Ar^+ , a mass increment of 1 AMU in an ion beam of decaborane will correspond to a displacement $\Delta x = 0.3" / 2.93 \approx 0.1"$. Thus, a wire of 0.06" dia was chosen for obtaining a better mass resolution with decaborane.

The argon beam profiles were measured at the image distance of the magnet since the magnet focuses the beam at this point. However, no substantial variation in the beam profiles due to spreading of the beam was observed when the measurements were taken at the sample chamber 10" away from the image distance.

3.3 Argon Beam Profiling in the Vertical Plane

The current distribution of the ion beam in the vertical plane was measured to estimate its effect on the dose of ions implanted into a sample. A metal strip of 0.2" width and 2.25" in height was traversed in the vertical direction in the path of the beam in discrete steps. The ion current was measured on the metal strip for each step and a plot of ion current vs. micrometer position for the vertical direction was made as shown in Fig. 3.6. In this experiment, the Ar^+ energy was 9 keV. It was seen that the ion beam is almost constant in the y-direction and the variation of the current within 0.5" around the maximum value is

less than 5 %. It was concluded from these measurements that for implantation into a small sample ($0.5'' \times 0.5''$) only a horizontal beam scanning will be necessary.

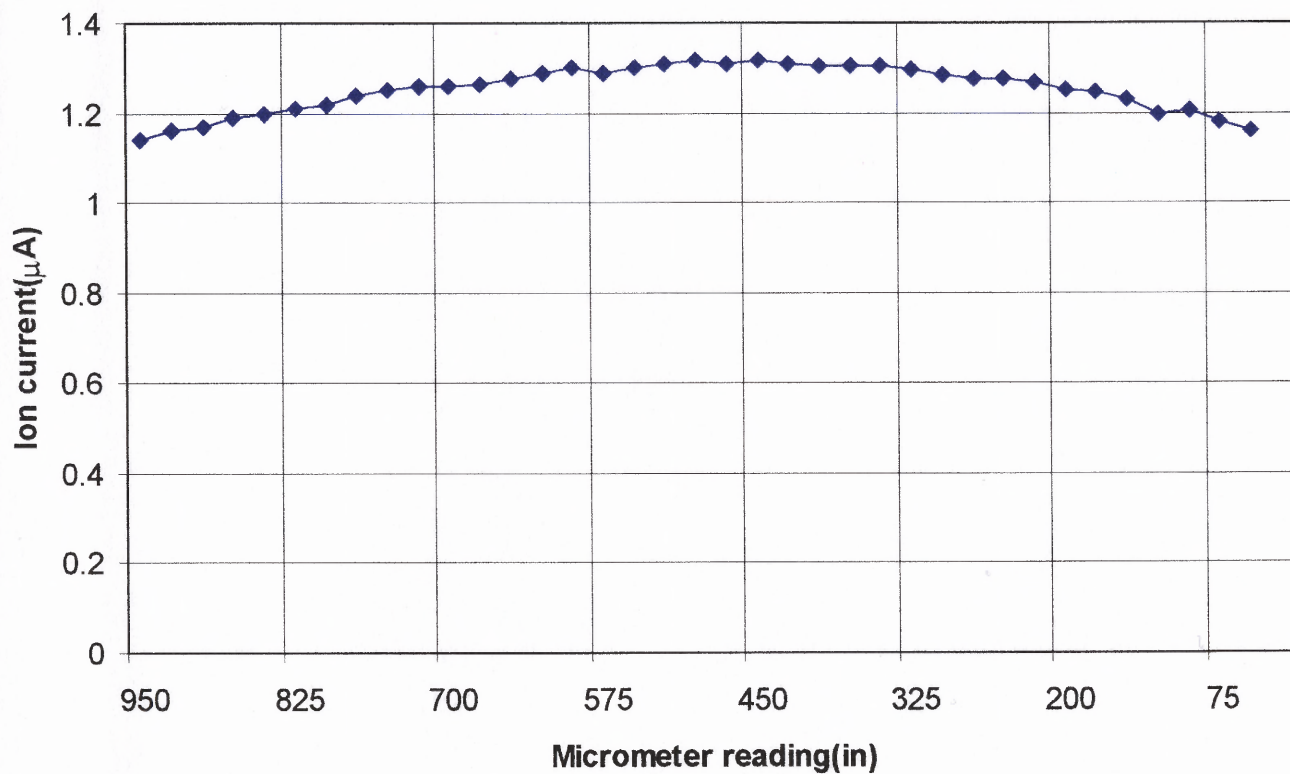


Fig. 3.6 Micrometer Scanned Profile of Ar^+ Ion Beam at 9 keV in the Vertical Direction

CHAPTER 4

EXPERIMENTS WITH DECABORANE ION BEAM

The functionality of the research implanter was tested and it was shown that it could be used for producing and transporting ion beams of argon, as described in Chapter 3. Similar experiments were done using decaborane vapor, and the resulting decaborane ion mass spectrum was compared with previous measurements with quadrupole mass spectrometer. Implantation and deflection experiments were done in order to test the feasibility of implanting decaborane in Si, to test for the possibility of vapor phase boron transport, neutral beam component and breakup of the B_{10} ions. Also, measurements of the size of the decaborane beam were carried out in order to establish the aperture width for implantation experiments.

4.1 Ionization of Decaborane and Decaborane Spectra

To understand the effects of electron impacts on the decaborane molecules, measurements of mass spectra of ions generated by impacts of electrons in the energy range from 20 eV to 250 eV and source temperatures up to 350°C were previously performed*. A mass spectrometer system consisting of an electron impact source, a quadrupole mass analyzer and an electron multiplier detector was used in the experiment and the resulting mass spectrum that was obtained at 70 eV and 250°C is shown in Fig. 4.1. These experiments established the electron energy of around 80 eV where the

* These measurements were performed as a part of a Masters thesis [10] and the results were previously reported.

B_{10} ions are most abundant although the relative abundance of B_{10} ions is minimum for this energy [7,10].

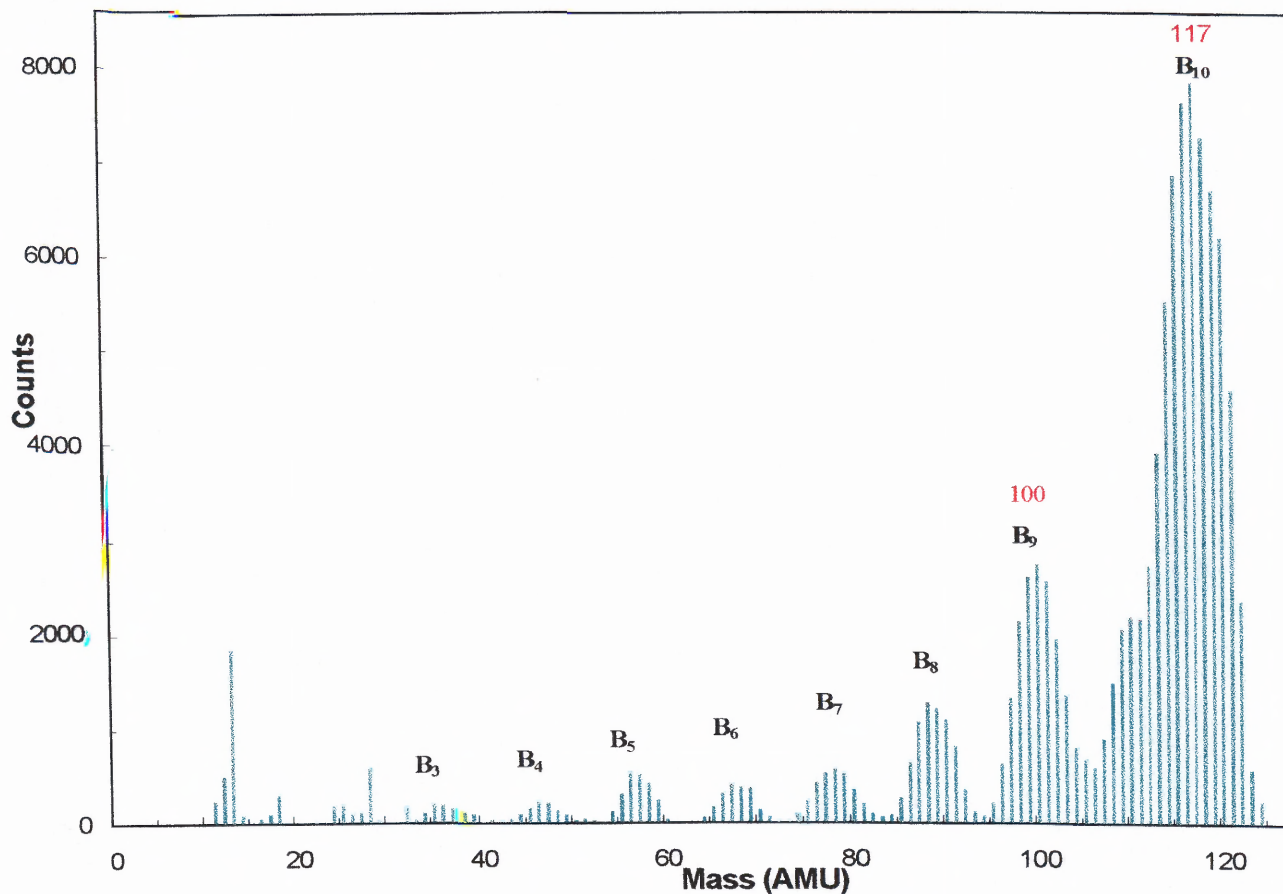


Fig. 4.1 Mass Spectrum of Decaborane

In the present work, ion mass spectra for decaborane in the energy range of 2 keV to 8 keV were obtained with the research ion implanter described in Chapter 2. Decaborane vapor generated by the process of sublimation was allowed to enter the ion source by opening the shut-off and needle valves while the argon inlet was shut off. Typical operation conditions for the source were filament current 2.2 A and anode voltage 80 V. Typical extraction and focussing conditions for ion energy of 4 keV were extraction voltage -230 V and focussing voltage -1450 V. The electron current observed for this

setting was approx. 10 mA and the typical source operating pressure was 1.5×10^{-5} torr. Details of obtaining the ion beam spectrum and ion current measurement using LabVIEW™ are given in Appendix-B. The ion mass spectrum was obtained at the focal point of the magnet by measuring ion current on a wire probe of 0.06" dia. The spectrum, after conversion of the x-axis to AMU from the calibration curve of the magnet, is shown in Fig. 4.2. The peaks corresponding to B_{10} , B_9 , B_8 and so on are easily identified on comparison with Fig. 4.1. Calculation of integrated B_{10} current under the B_{10} peak is dealt with in Section 4.2.

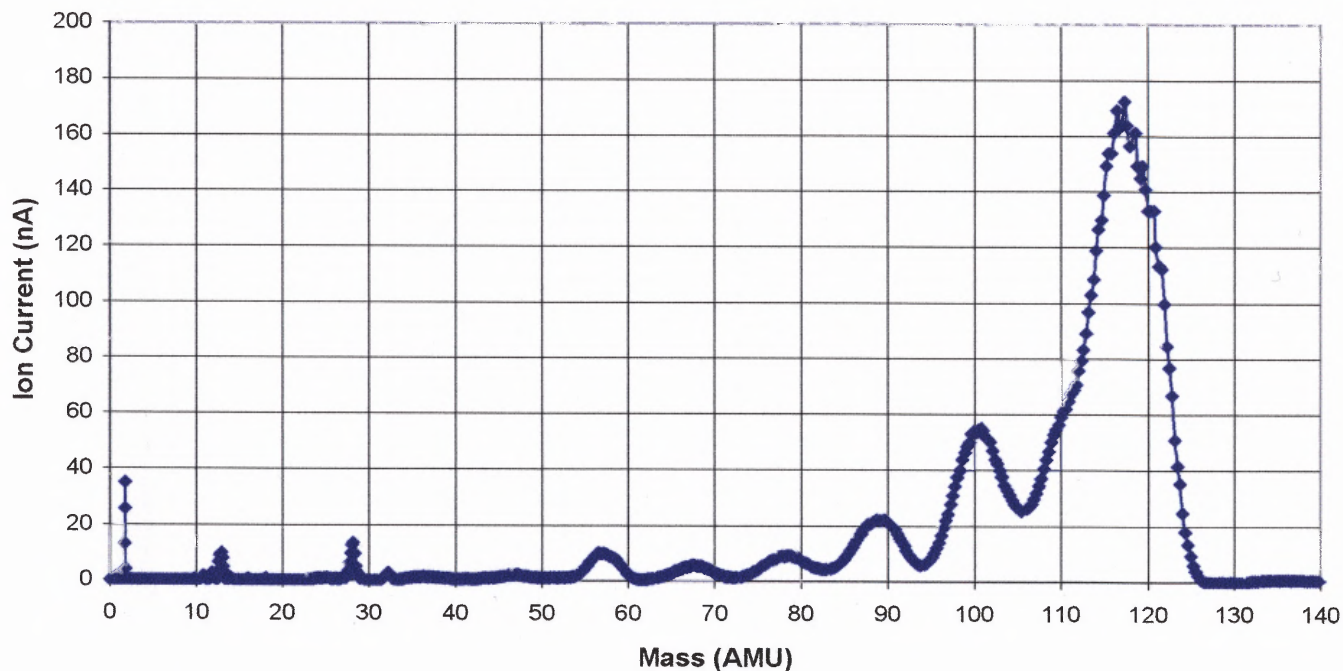


Fig. 4.2 Mass Spectrum of Decaborane on Wire Probe at 6 keV

4.2 Integration of B₁₀ Ion Current

The total (integrated) decaborane ion current under the B₁₀ peak is an important parameter in estimating the time of decaborane implantation. The integration procedure has to take into account the fact that the magnet current increments correspond to the mass increments smaller than the mass resolution defined by the used probe wire diameter of 0.06". Thus, two factors namely Δm_{step} (incremental change in mass due to increase in magnetic field) and Δm_{probe} (the mass interval as defined by the probe wire diameter) have to be considered in integrating the ion current. The current values are normalized by multiplying each value of current by the ratio $(\Delta m_{step} / \Delta m_{probe})$, and a simple summation of the resulting values results in the integrated B₁₀ current. Here, $\Delta m_{step} = (dm/dB) \Delta B$ where ΔB is the magnetic field increment. $\Delta m_{probe} = (dm/dx) a$ where a is the probe wire diameter.

Now, $(dm/dx) \sim m$, which follows from Eq. (3.1). Thus, $(dm/dx) = (k) m$ where k is a constant of proportionality depending on the characteristics of the magnet. In our case, $k = 0.073$ was obtained from Eq. (3.1). Therefore, $\Delta m_{probe} = (k) m a$. For the probe wire diameter of 0.06, $\Delta m_{probe} = 0.004 m$.

Also, $(dm/dB) \sim B$, $\sim m^{1/2}$, which follows from Eq. (2.1). Therefore, $\Delta m_{step} \sim m^{1/2}$ because the magnetic field increment in our experiments was constant (2.55×10^{-4} T) as the magnet current was incremented in equal steps defined by the control circuit and the LabVIEW™ program. Using Eq. (2.1) to obtain (dm/dB) and using ΔB of 2.55×10^{-4} T, we get $\Delta m_{step} = (1.94 / \sqrt{V_{ext}}) m^{1/2}$ where the factor 1.94 is the constant of proportionality and V_{ext} is the potential through which ions are accelerated in volts.

Using the normalizing factor of $(\Delta m_{step}/\Delta m_{probe})$ for each B_{10} ion current value, the resulting integrated B_{10} current for the spectrum shown in Fig. 4.2, is $3.3 \mu\text{A}$. In the decaborane ion spectrum obtained on the 1.12" wide sample block as shown in Fig. 4.3, each point represents the decaborane current integrated over the block width. The maximum current for the B_{10} peak in the spectrum shown is $2.15 \mu\text{A}$. This difference is explained by the fact that the decaborane beam is spread wider in the x-direction than the sample block, as is discussed in Section 4.3.

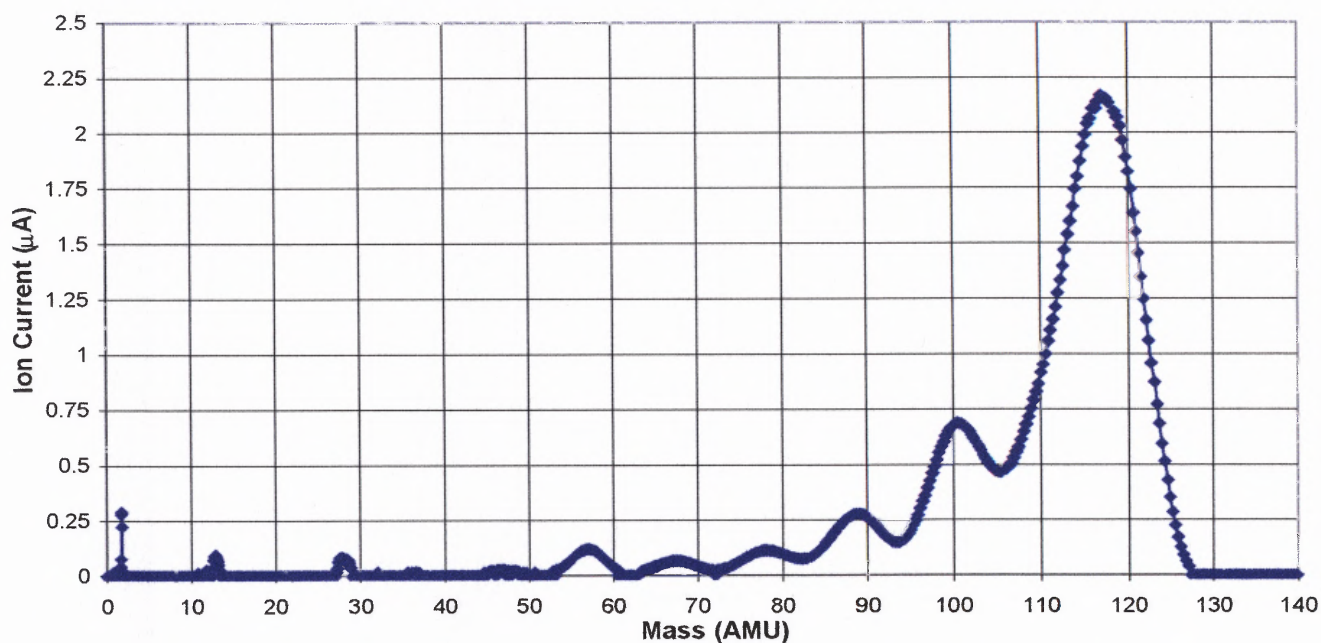


Fig. 4.3 Mass Spectrum of Decaborane on Sample Block at 6 keV

4.3 Beam Profiling of Decaborane Ion Beam

Beam profiling of the B_{10} ion beam was done at the focal distance of the magnet in order to understand the current distribution and also to establish the width of the aperture required for allowing a given number of ion masses to be implanted in Si. The selection of the aperture width also determines the effective ion current obtained with a scanned beam.

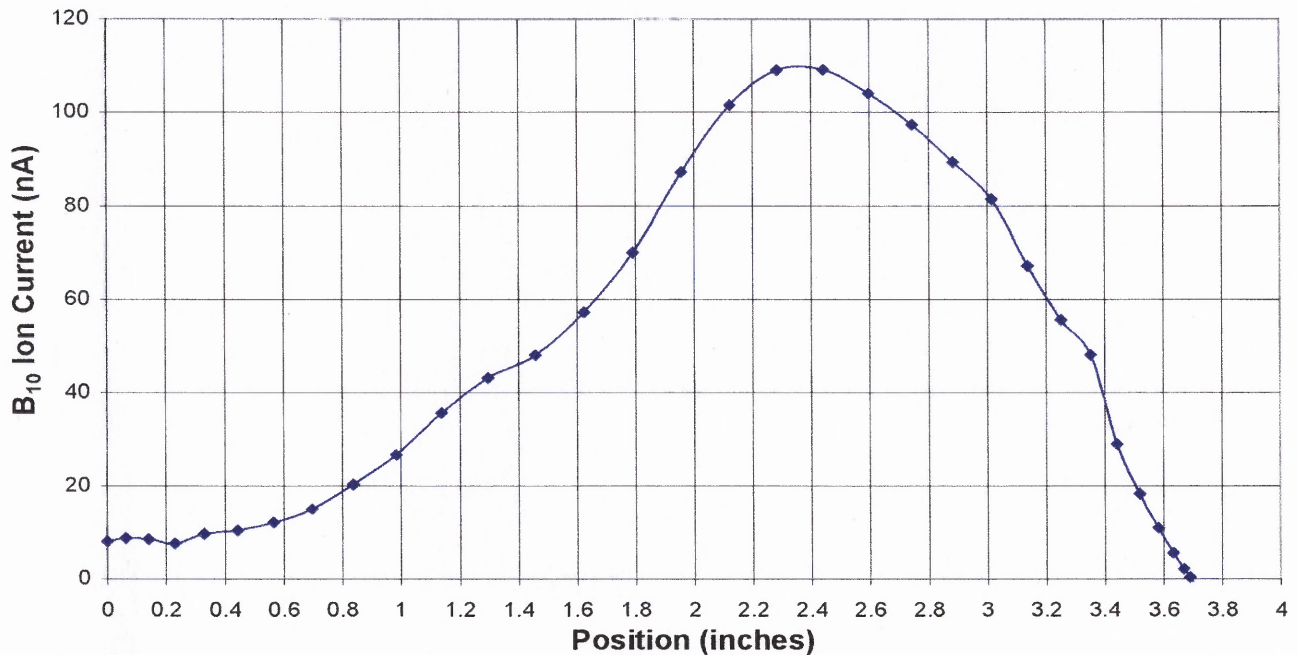


Fig. 4.4 Scan of B_{10} Ion Beam along Horizontal Axis Perpendicular to the Beam

A wire of 0.06" dia, which was mounted with an offset of 1.9" from a similar wire at the center (as shown in Fig. 2.6), was rotated along a circular path in the B_{10} ion beam in steps of 5° . Ion beam current was measured for each step and a graph of ion current vs. angular displacement was obtained. Converting the x-axis from angular displacement to linear displacement, a plot of ion current vs. linear displacement was obtained as shown in Fig. 4.4. From the above graph, the width of the B_{10} peak at half maximum is 2.25". The variation of the percentage of total B_{10} ion current for different aperture widths

(integrated current under a given aperture width) is plotted as a curve shown in Fig. 4.5. This curve is useful for arriving at the optimum aperture width for implantation. The graph shows that with the aperture width of 1", 50 % of total B_{10} current is obtained while increasing the width to 1.5" results in almost 70 % of the total B_{10} current. It can be inferred from the above that the integrated current on the 1.12" block width is 55 % of the total B_{10} current.

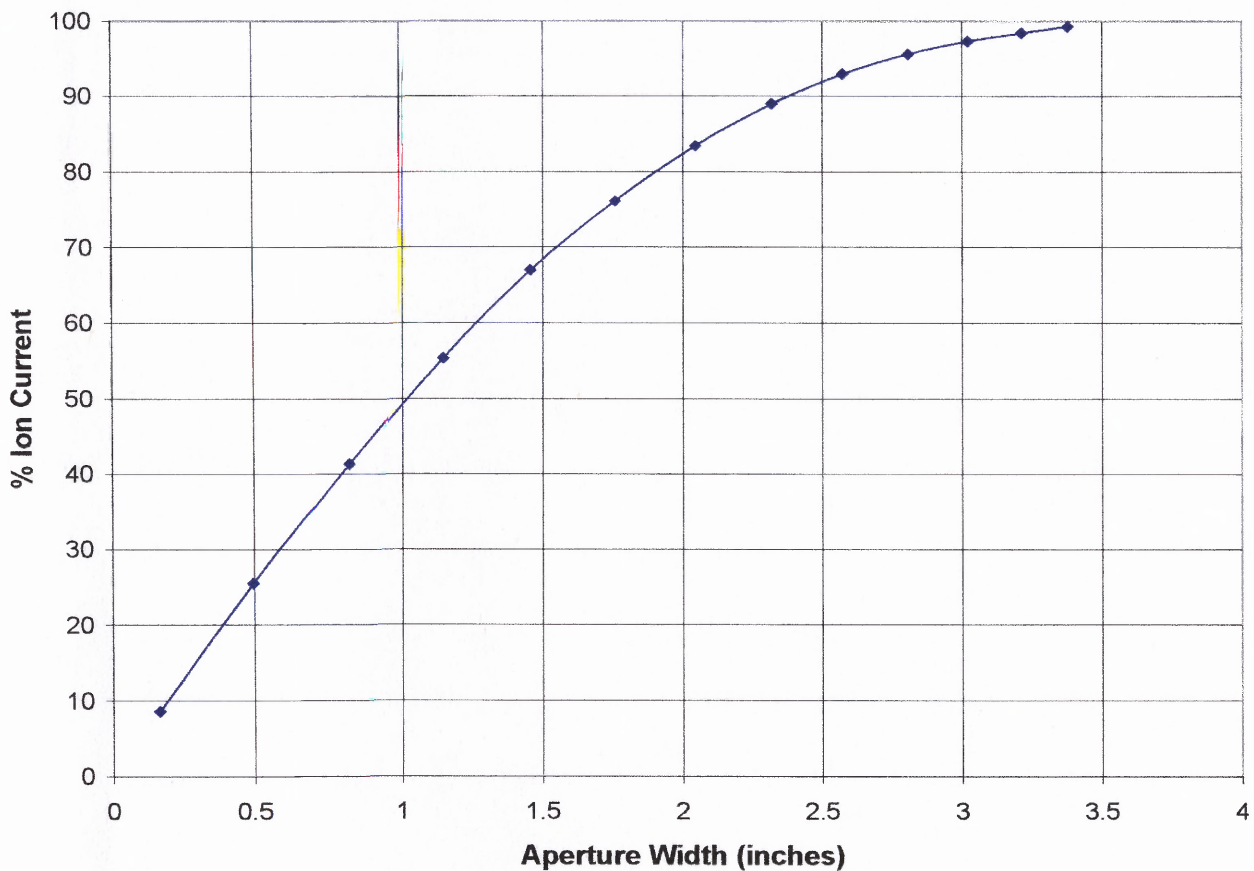


Fig. 4.5 Fraction of Total B_{10} Current vs. Aperture Width

Since the integrated current on the block is $2.15 \mu\text{A}$ as seen from Fig. 4.3, the total B_{10} current should be $3.9 \mu\text{A}$. The difference between this value and the value of $3.3 \mu\text{A}$ obtained by the method of integration of current described in Section 4.2, can be

attributed to the reduction in the ion current measured by the wire due to absorption secondary electrons emitted from the block, as will be described in Section 4.5.

4.4 Decaborane Implantation with Deflection and NRA

A combination of ion beam deflection and implantation experiment in silicon was set up to study the following issues related to the B_{10} ion beam.

- 1) Feasibility of implanting decaborane in Si
- 2) Breakup of the B_{10}^+ ions in the beamline after the magnet
- 3) Existence of energetic neutrals in the ion beam
- 4) Vapor phase transport of decaborane on Si.

4.4.1 Electrostatic Deflection of Decaborane Beam and Implantation

The experimental setup is schematically represented in Fig. 4.6. The decaborane ion

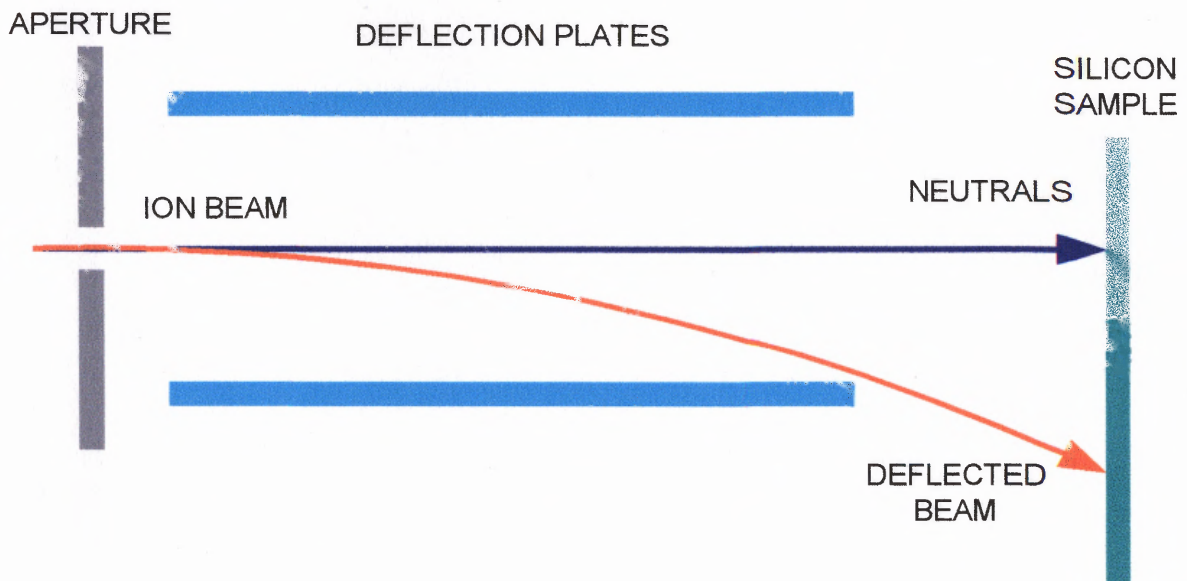


Fig. 4.6 Implantation Experiment with Deflection

beam with energy of 4 keV was passed through an aperture of 0.1" and incident on a silicon sample with crystal orientation (100) and having dimensions 2.0" \times 0.66". The beam was deflected by applying appropriate voltage on the deflection plates so that the ions were implanted into the Si sample 1.2" from the center of the undeflected ion beam path. The neutral component of the beam will pass undeflected between the plates and will be implanted at the center of the Si sample. Any B₁₀ ions that break up after the magnet will be implanted in the sample in the region between the center of the sample and 1.2" from the center of the sample. The magnitude of voltage to be applied on the plates was found to be 230 V for a deflection of 1.2" using Eq. (2.2). In order to test vapor phase transport of decaborane, another Si sample was mounted on the sample block and was not exposed to the ion beam during the implant time of 25 min. The implant dose was chosen as 1×10^{14} B₁₀ ions/cm², which is equal to 1×10^{15} boron ions/cm². For details regarding dose measurement refer Appendix-B.

4.4.2 Nuclear Reaction Analysis and Results

The presence of boron in the implanted sample and in the sample not exposed to the ion beam was determined using Nuclear Reaction Analysis (NRA) carried out at Bell Labs, Murray Hill, NJ. The schematic of the NRA is shown in Fig. 4.7. A 650 keV beam of protons is incident on the Si sample. α particles are emitted due to the reaction $^{11}\text{B} + ^1\text{p} \rightarrow ^8\text{Be} + ^4\alpha$, and are counted by a solid state detector. The Mylar foil is used to stop scattered protons. The number of α particles emitted is proportional to the Boron concentration in the sample.

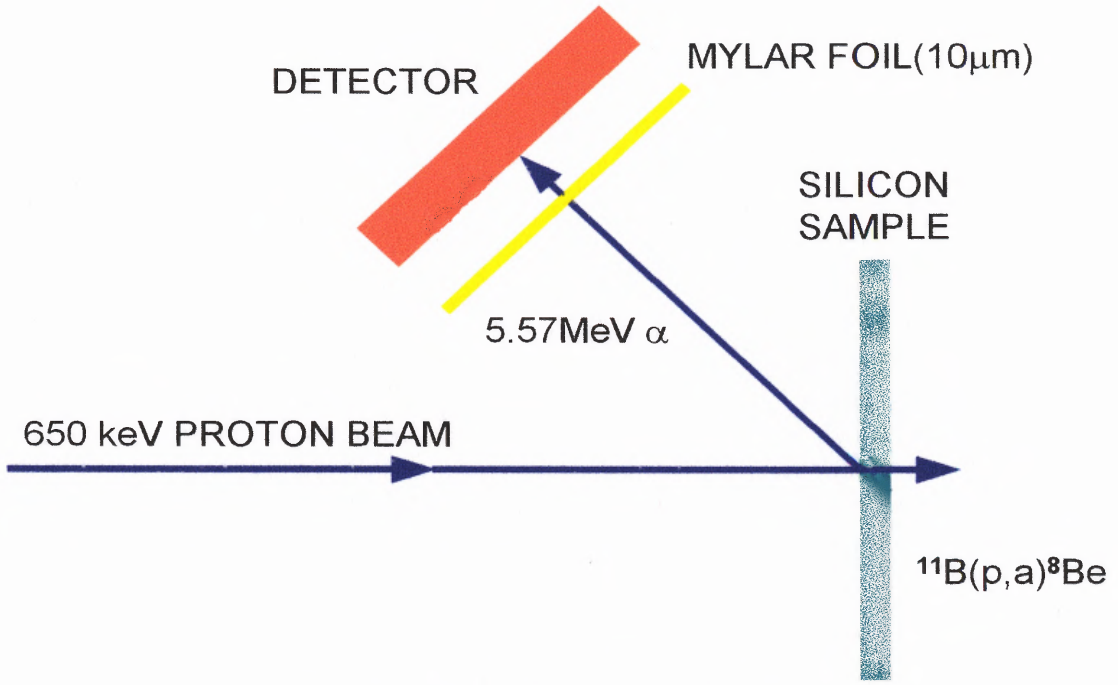


Fig. 4.7 P- α Experimental Setup

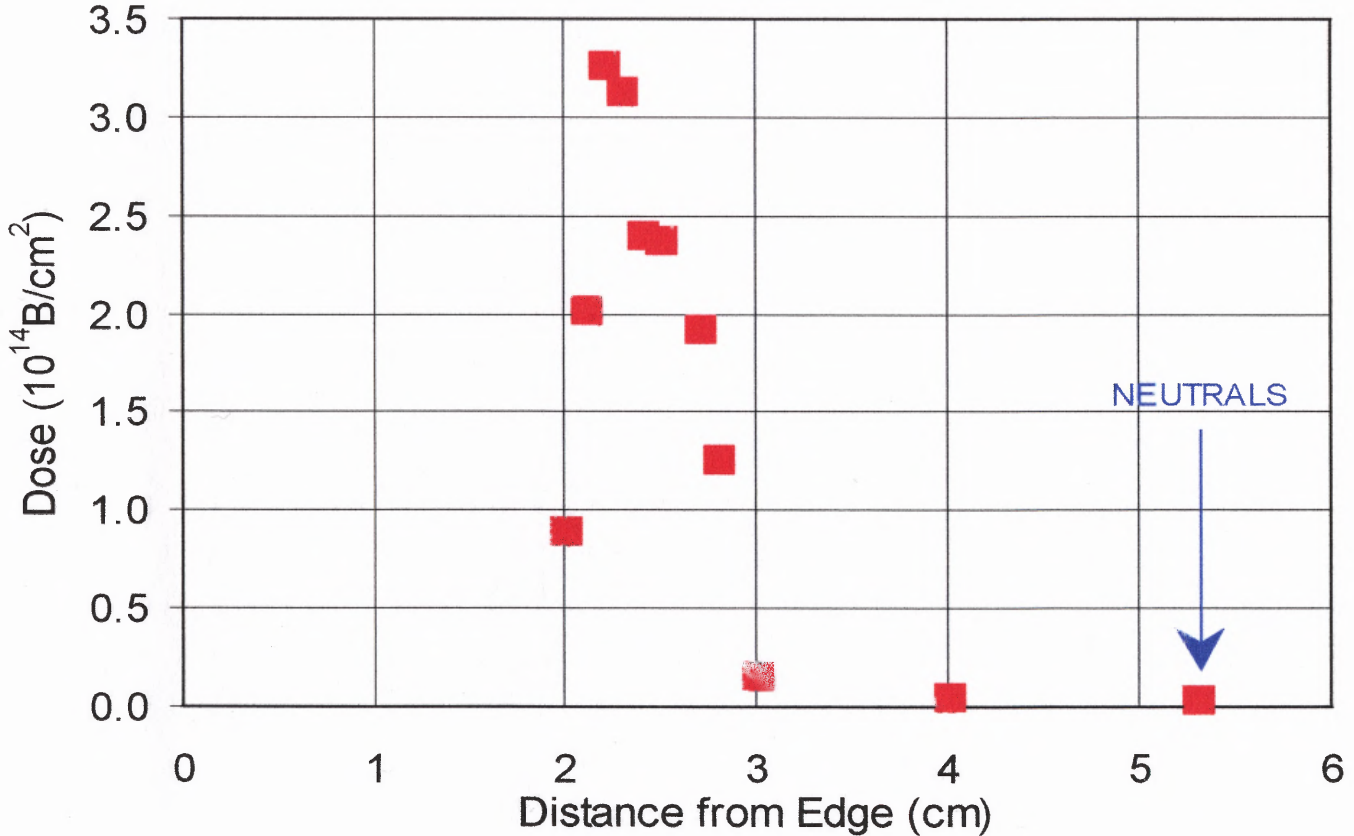


Fig. 4.8 Variation of Boron Dose on the Sample

The proton beam was scanned along the sample in 1 mm steps, and a profile of boron dose vs. beam position on the sample was obtained, as shown in Fig. 4.8. The number of counts measured at the neutral beam position was 4.31×10^{12} or $\sim 1\%$ of the 3.28×10^{14} counts at the maximum dose position (1.2" from center of the sample). At the intermediate position between the neutral beam position and the maximum dose position, the number of counts measured was 6.47×10^{12} counts or $\sim 2\%$ of the counts at the maximum dose position. The sample that was unexposed to the beam was also subjected to NRA, and the number of counts obtained was approximately equal to the counts obtained when an unimplanted reference sample was subjected to NRA.

The following was concluded from the above, after considering the background noise for NRA:

- 1) Break up of the B_{10} ions after the magnet is less than 2 % of the maximum implanted dose.
- 2) Neutral beam component is less than 1% of the maximum implanted dose.
- 3) There is no appreciable vapor phase transport of decaborane in the system.

4.5 Implantation Experiments with a Scanned Decaborane Beam

Implantation experiments in Si were carried out with a scanned decaborane beam for obtaining uniform dose distribution over the sample. An aperture of length 0.9" and height 0.75" was chosen to obtain $\sim 50\%$ of the total B_{10} ion beam and was mounted at the focal distance of the magnet, 0.5" before the deflection plates.

A major problem in determination of an implanted ion dose arises from the presence of secondary electrons generated by an impact of energetic ions. There are two main sources of dose errors namely:

- 1) Secondary electrons that escape from the sample when high-energy ions strike the sample. In this case, every electron escaping from the sample is wrongly counted as an implanted ion.
- 2) Secondary electrons that are generated when the high-energy ion beam strikes the edges of an aperture and are incident on the sample. In this case, every incident electron on the sample reduces the number of counted implanted ions by one.

To guard against dose errors due to secondary electrons, an electron suppressor structure consisting of two apertures was mounted in front of the sample block. The first aperture, a $0.8'' \times 0.8''$ square, was mounted $1.5''$ after the deflection plates and was at ground potential. The second larger aperture, a $1.2'' \times 1.2''$ square, was electrically isolated from the first aperture by ceramic insulators of $0.75''$ length. The second aperture was at a distance of $2.5''$ from the sample. By application of a negative voltage of an appropriate magnitude on the second aperture, secondary electrons from the first aperture are repelled and are prevented from entering the sample chamber. At the same time, secondary electrons ejected from the sample are repelled back to the sample. Experiments were done with decaborane where the second aperture was biased with a negative voltage that was increased in steps. For each step, the current was measured on the sample block and a graph was obtained at 4 keV, as shown in Fig. 4.9.

From the graph, it is seen that a negative suppression voltage of magnitude greater than 100 V results in a reduction in the ion current by ~35 % because secondary electrons are prevented from escaping from the sample block.

First implantation experiments were performed with scanning in the horizontal direction only. A suppression voltage of -500 V, deflection voltage of ± 300 V and a scanning frequency of 500 Hz were used.

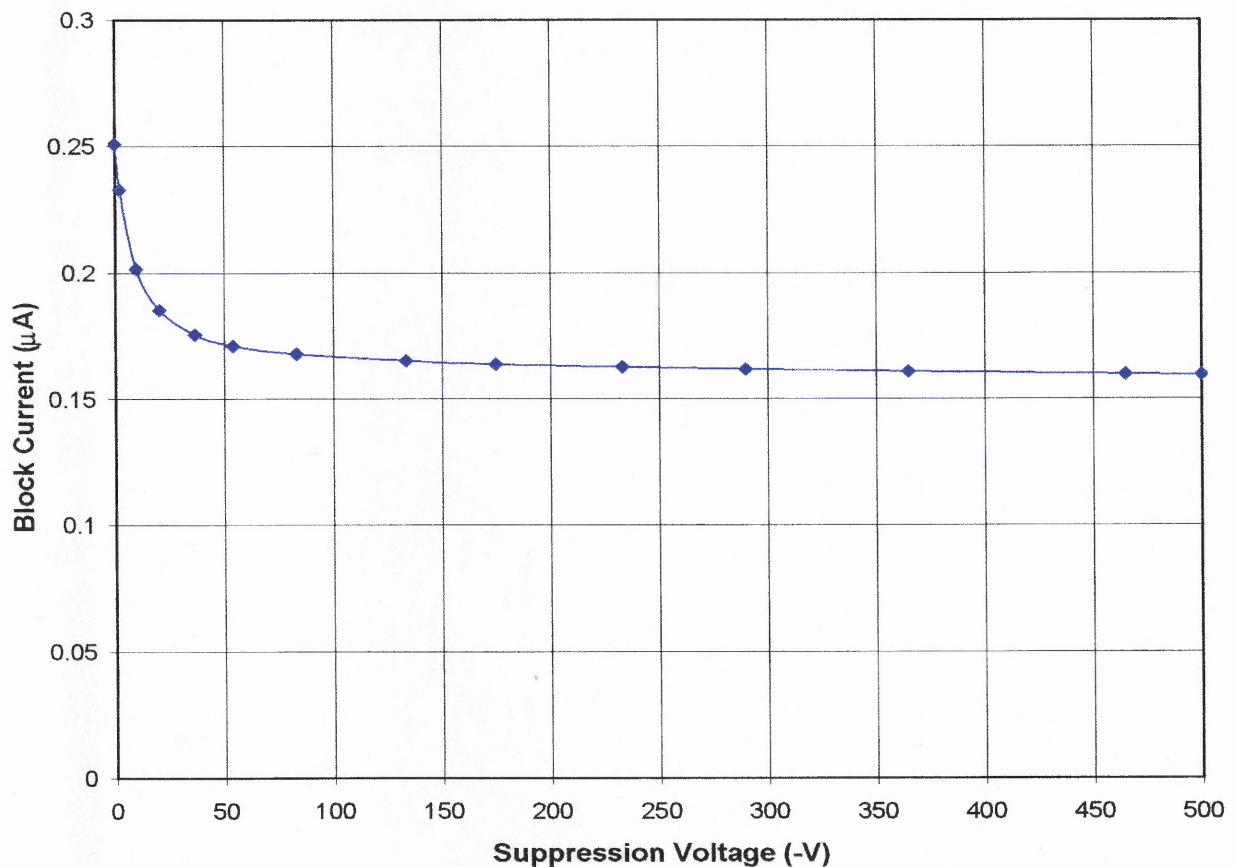


Fig. 4.9 Variation of Beam Current vs. Aperture Voltage

The dose of the implanted sample was measured using NRA, as described in Section 4.4.2. The proton beam was scanned in 2 mm steps in the vertical and horizontal directions along the sample. The average dose measured in the vertical direction was

3.9×10^{15} boron ions/cm² while the average dose measured in the horizontal direction was 4.8×10^{15} boron ions/cm². The average dose over the sample was calculated as the mean of the average doses in the vertical and horizontal directions as 4.4×10^{15} . This agrees within 7 % of the implanted dose of 4.11×10^{15} , by ion current integration. This value of 7 % is reasonable, considering the statistical error of more than 2 %* in NRA, the method of averaging used and the absence of vertical electrostatic beam scan. It is expected that this value will be reduced by improvements in the electron suppression system or by the addition of vertical scanning, which should improve the averaged dose uniformity on the sample.

* Statistical error in NRA varies as the square root of number of acquired counts. In this case, average number of counts acquired during NRA for the vertical and horizontal scans was ~ 2000.

CHAPTER 5

SUMMARY AND CONCLUSIONS

The course of work on this thesis is summarized in the following sections.

- **Construction of Beamline**

The beamline of the research ion implantation system was designed and built. A vacuum system with three turbo-molecular pumps that allow independent venting of different beamline sections, and a gas handling system that provides control of decaborane vapor and the argon gas flow to the source, were designed and constructed.

- **Development of Electrical System / Hardware**

A control circuit for the magnet power supply was designed and built that provides a manual setting of a given magnetic field and an external input for computer control. Special current integrator and timer instruments were calibrated and interfaced to provide accurate dose control for implantation and also for data acquisition. High voltage power supplies were set up for beam scanning and secondary electron suppression.

- **Control and Data Acquisition / Software**

Programs were developed for automated control of magnet power supply and also for data acquisition using DAQ and GPIB interfaces using LabVIEW™. Beam trajectory, deflection and focussing effects were studied using SIMION.

The experimental results and conclusions are summarized in sections 5.1 and 5.2.

5.1 Experiments with Argon

- 1) Tested the functionality of the implanter using argon ions.
- 2) Found that the width of Ar^+ beam is approx. 0.3" and is focussed in the horizontal plane (ion current variation of less than 5 % in the vertical plane).
- 3) Calibrated the magnet by using the values of magnet current for Ar^+ and Ar^{++} ions.

5.2 Experiments with Decaborane

- 1) Obtained an ion beam of decaborane with a maximum ion current in the order of a few microamperes on the sample block.
- 2) Obtained the ion mass spectrum of decaborane and found to be in agreement with previously obtained measurements using a mass spectrometer.
- 3) Implanted deflected B_{10} ions in Si, and concluded the following after considering the background noise for NRA.
 - Break up of the B_{10}^+ beam in the beamline after the magnet is less than 2 % of maximum implanted dose
 - Neutral component in the beam is less than 1 % of maximum implanted dose
 - There is no appreciable vapor phase transport of decaborane in the system
- 4) Implanted B_{10} ions in Si samples with horizontal electrostatic scanning, with an agreement within 7 % of the implanted dose, by ion current integration.

In the next phase of this research program, the characteristics of Si implanted with decaborane ions will be investigated. An important issue, which is Transient Enhanced Diffusion (TED) that occurs due to thermal annealing and decides the final junction

depth, will be studied and compared with samples implanted with boron. Other effects such as crystal damage, amorphization and sputtering will be studied using characterization techniques such as RBS (Rutherford Back Scattering), NRA (Nuclear Reaction Analysis), TEM (Transmission Electron Microscopy) and SIMS (Secondary Ion Mass Spectroscopy).

APPENDIX A

DECABORANE

Decaborane is the largest and the most stable among the boron hydrides. In this section, general information regarding the structure, physical and chemical properties of decaborane and most importantly the safety aspects to be taken care of while handling decaborane are described.

- **Structure, Physical and Chemical Properties**

Decaborane molecule comprises a cage of ten covalently bonded boron atoms with a hydrogen atom bonded to each of them. The remaining four hydrogen atoms form single-atom bridges between four pairs of ten boron atoms. Thus, most of the boron-boron bonds in the compound do not involve any hydrogen bridging. The average boron-boron bond distance in the molecule is 1.77 A.U but each boron atom forms part bonds at various distances with its boron atom neighbors [24].

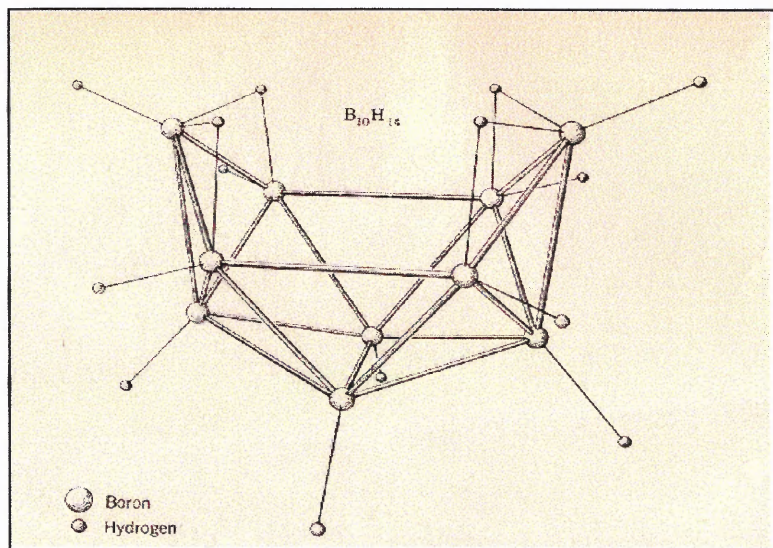


Fig. A.1 Structure of Decaborane Molecule

Table A.1 Properties of Decaborane

Formula	$B_{10}H_{14}$
Molecular Weight	122.31
Description of Substance	Colorless to white crystalline solid with an intense, bitter, chocolate-like odor.
Melting Point	$99.7^{\circ}C$
Boiling Point	$213^{\circ}C$
Density	0.94 g/cc at $20^{\circ}C$
Vapor Pressure	0.15 torr at $20^{\circ}C$, 19 torr at $100^{\circ}C$.
Heat of Sublimation	19.4 kcal/mole.

Decaborane is stable indefinitely at room temperature. In absence of air, it can be heated to $150^{\circ}C$ for extended periods without decomposition. It decomposes only slightly in 48 hrs at $200^{\circ}C$. Decomposition to hydrogen and a solid composition $B_nH_{0.6n}$ is complete in 25 hrs at $250^{\circ}C$, but decomposition into boron and hydrogen is very slow at $300^{\circ}C$.

- **Material Handling and Safety**

Decaborane is a toxic substance, comparable in this respect to diborane, not less so than pentaborane [24]. Poisoning by decaborane can occur by inhalation, absorption through skin or ingestion, although the possibility of exposure can be minimized by ordinary protection of the skin, the eyes, and the respiratory system. Any decaborane that is splashed or spilled on a person must be thoroughly washed from the affected skin and

eyes. Areas containing toxic concentrations of decaborane vapor must be evacuated at once. Whenever there is any kind of decaborane exposure, a physician should be summoned immediately.

Decaborane reacts with natural rubber and destroys latex on contact; buna-nitrile gloves should be used. For cleaning of parts, alcohol can be used, followed by a water rinse. A scrubber with active carbon is effective for decontamination of exhaust from vacuum pumps. Areas spilled with decaborane can be decontaminated with methanol; aqueous ammonia has also been suggested.

Several methods have been developed for the detection and determination of decaborane. It can be determined by ultra-violet spectroscopy in aqueous triethanolamine solution or colorimetrically from its red adduct with quinoline. Neither diborane nor pentaborane interfere with these methods nor with a calorimetric method based on the orange red solution formed with N, N-diethylnicotinamide. Matheson Kitagawa toxic gas detection tubes are used for detection of decaborane. Although the tubes are calibrated for arsene, they are found to detect decaborane as well.

APPENDIX B

MAGNET CONTROL AND DATA ACQUISITION SYSTEM USING A COMPUTER WITH LABVIEW™ SOFTWARE

The control and data acquisition system is built around a PC with a Data Acquisition (DAQ) card and an IEEE STD 488-interface or General Purpose Interface Bus (GPIB) card. A computer-controlled system has the following advantages:

- 1) Time taken for obtaining the spectrum is much less when compared with the time taken to obtain the same spectrum manually.
- 2) The data can be stored in the form of computer files, which facilitate analysis and graphic representation.

Control of the magnet is achieved with the help of a circuit producing a control voltage to the magnet power supply, which is adjusted either manually or by a signal from the DAQ board. The magnet current is obtained by measuring the voltage across a $0.33\text{ m}\Omega$ high-power resistor that is connected in series with the coils of the magnet, by using a FLUKE 8840 multimeter equipped with an IEEE 488 interface. The ion current is measured by connecting a wire probe or the sample block that picks up the ion current to a pico-ammeter (Kiethley Model no. 6904B) through a coaxial cable with BNC connectors. The pico-ammeter has an analog output that can be read by the DAQ board. Alternatively, an EG & G ORTEC digital current integrator is used for providing a digital output, which is read by the DAQ card.

B.1 Control Circuit for the Magnet

A Hewlett Packard 6269B power supply operating in the constant current mode is used to supply current to the magnet [18]. The magnet power supply is operated in one of the following modes:

- Resistance programming of the magnet current

Resistance programming of output current has a resolution of $1 \text{ A}/4 \text{ } \Omega$. A $240 \text{ } \Omega$ potentiometer connected to designated terminals of the magnet power supply is used to control the output current.

- Voltage programming of the magnet current

Voltage programming of the magnet current is used for better resolution and greater stability with time and temperature as well as for convenience of using a computer control circuit. The HP6269B supplies a maximum current of 60 A for a control voltage input of 600 mV.

A control circuit for the magnet power supply allows manual setting of the magnetic field using a potentiometer (DC offset) and also an external control input from a computer. The circuit is schematically represented in Fig. B.1.

A LM324N general-purpose quad OPAMP is used to implement voltage followers for the inputs, a summing amplifier and an inverter at the output. Two OPAMPS in the general-purpose quad OPAMP LM324N are used as buffers in the non-inverting mode for the DC offset input and the external input. A LM 338Z 2.3 V linear voltage regulator is used to obtain a regulated DC control input that is varied using a coarse 0-25 k Ω , 10-turn potentiometer and a 240 Ω , 10-turn potentiometer for fine

adjustment. The DC and the external control inputs are combined using a summing amplifier.

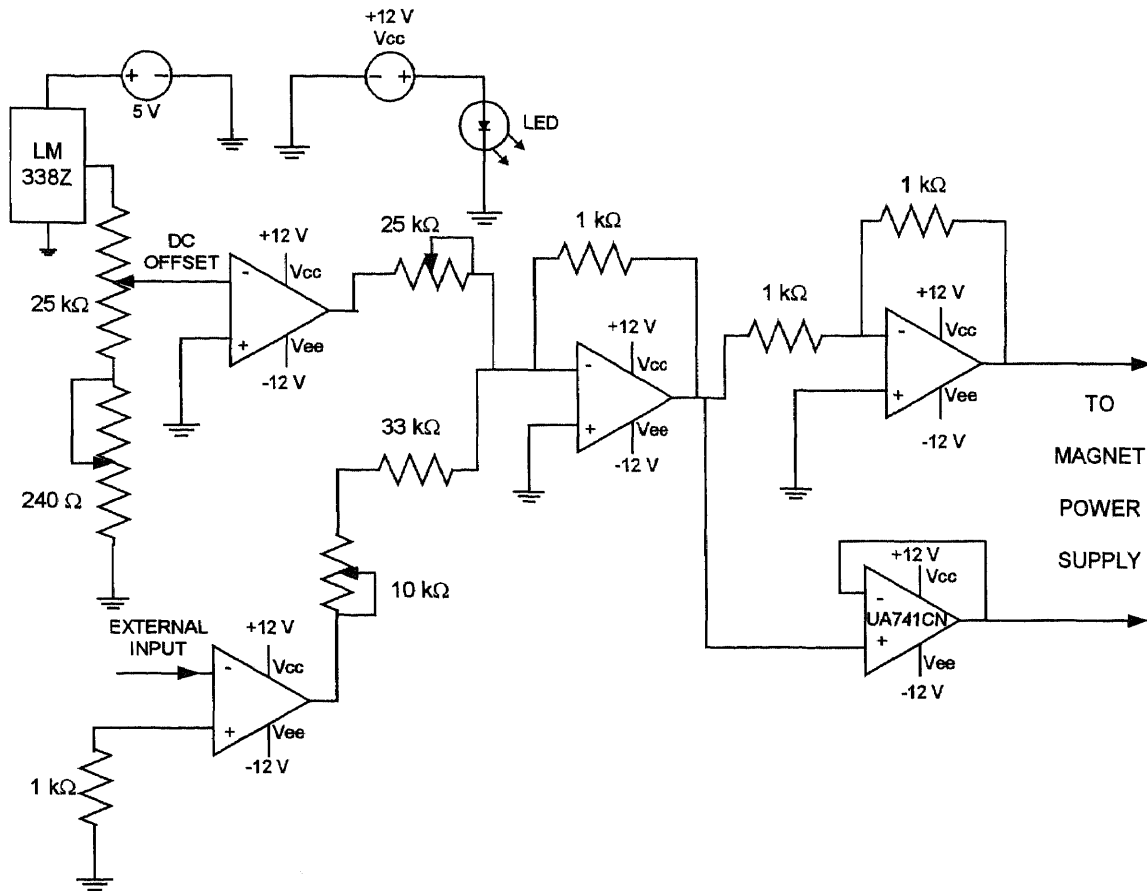


Fig. B.1 Control Circuit for Magnet Power Supply

The gain of the summing amplifier for the DC control input can be adjusted to the control input requirements of the magnet power supply by a trimming potentiometer of 10 kΩ. The fourth OPAMP in the quad package is used as a unity gain inverter for inverting the output of the summing amplifier. An additional general purpose UA741CN OPAMP is added in order to have two control inputs of opposite polarity to the magnet power supply that are isolated from ground. A Motorola ± 12 V (0.13 A), +5 V (0.5 A) DC power-

supply powers the circuit, which is mounted in an aluminum case that is grounded to the chassis of the magnet power supply.

B.2 LabVIEW™ Control and Data Acquisition

LabVIEW™ from National Instruments Corp. is a graphical programming development environment for data acquisition, analysis and control. LabVIEW™ gives the flexibility of a powerful programming language without the associated difficulty and complexity because its graphical programming methodology is inherently intuitive to scientists and engineers [20].

In LabVIEW™, programs are stored as Virtual Instruments (VIs). Front panel user interfaces can be quickly created, resulting in interactive control of the software system. On the front panel of the VI, controls and data displays for the system are placed by choosing objects from the Controls palette, that includes numeric displays, meters, LEDs, charts, graphs, and so on. The front panel is used to control the system while the VI is running such as by clicking on a switch or entering a value from the keyboard. To program the VI, a block diagram is constructed without worrying about the many syntactical details of conventional programming. Objects (icons) can be selected from the Functions palette and connected with wires to pass data from one block to the next. These blocks range from simple arithmetic functions, to advanced acquisition and analysis routines, to network and file I/O operations. Since the execution order in LabVIEW™ is determined by the flow of data between blocks, and not by sequential lines of text, diagrams can be created that have simultaneous operations. LabVIEW™ is a multitasking and multithreaded system, that runs multiple execution threads and multiple VIs.

LabVIEW™ VIs are modular in design, so any VI can run by itself or be used as part of another VI [21]. LabVIEW™ uses various functions to input or output analog/digital signals to the DAQ card and communicates with and controls external instruments such as oscilloscopes and digital multimeters using General Purpose Interface Bus (GPIB). The GPIB functions for LabVIEW™ follow the IEEE 488.2 specification. [25].

Automated control of the magnet power supply and data acquisition for obtaining the ion current spectra used DAQ and GPIB interfaces on a PC that runs LabVIEW™

4.1. The block diagram of the system is shown in Fig. B.2.

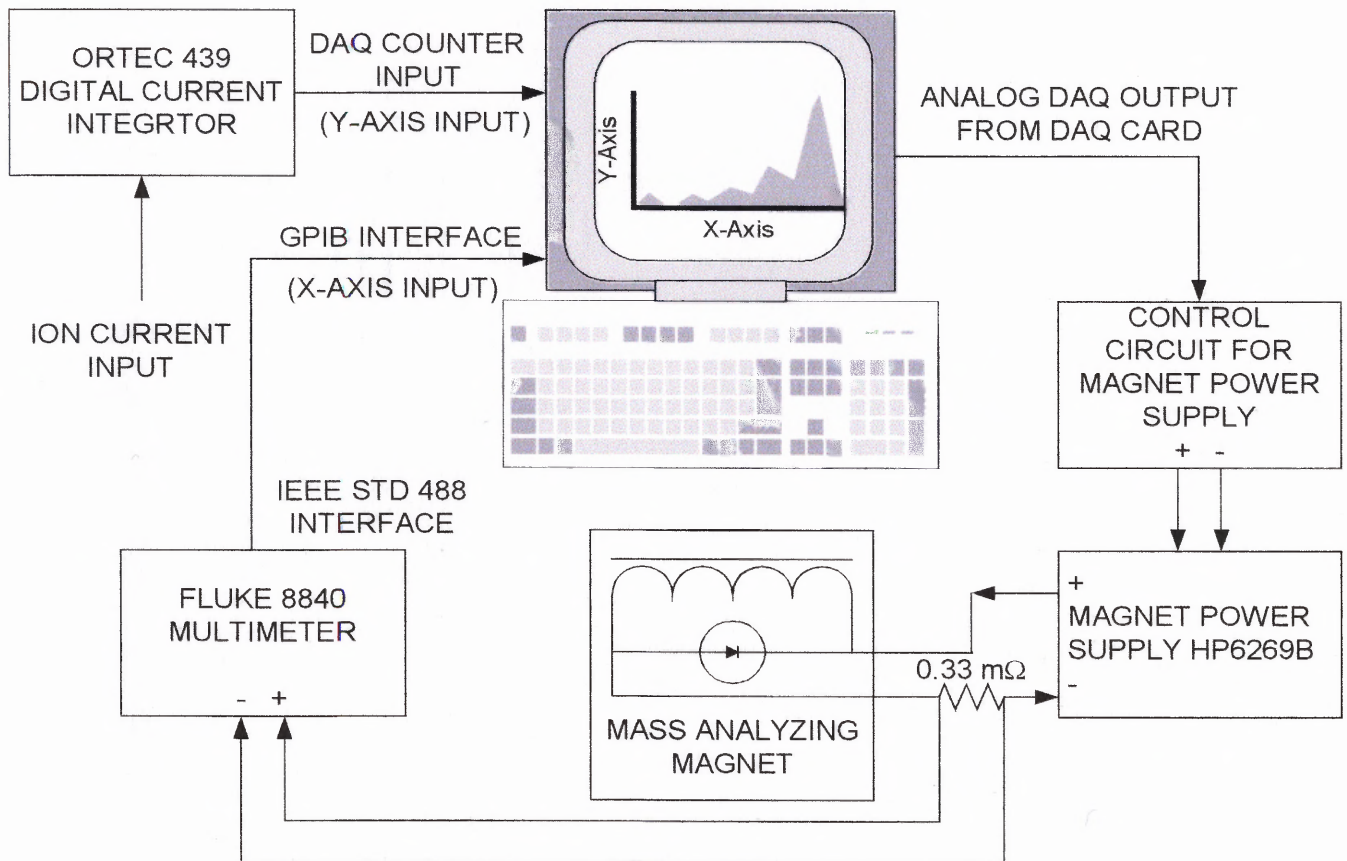


Fig. B.2 Block Diagram of Magnet Control and Data Acquisition

A FLUKE 8840 multimeter that has the IEEE STD 488 port is connected to a National Instruments NI-488.2M™ interface board for GPIB control [23]. The DAQ PCI E Series board generates steps of analog voltage to the control circuit of the magnet power supply, which in turn controls the current flowing through the coils of the magnet. The value of this current is obtained by measuring the voltage (which is proportional to the current) across a $0.33\text{ m}\Omega$ resistor connected in series with the magnet coils using a FLUKE 8840 multimeter, and this voltage value is referred to as “magnet setting” or “magnet reading”. This GPIB output from the FLUKE 8840 gives the x-axis value for the ion beam spectrum. The ORTEC 439 digital current integrator provides pulses with frequency that is proportional to the input ion current, based on the “coulomb/pulse” setting. The frequency measured by the DAQ PCI E Series board, is proportional to the ion current and gives the y-axis value of the spectrum.

The sequence of steps for obtaining an ion current spectrum using LabVIEW™ is represented by the flowchart shown in Fig. B.3. The minimum voltage step generated by the DAQ is 5 mV. The number of points for the spectrum is obtained by dividing the maximum magnet setting by 0.01, which is the change in the magnet reading in mV, for a DAQ output voltage change of 5 mV. The magnet setting step of 0.01 V for the control voltage step of 5 mV is determined by the gain of the summing amplifier in the control circuit for the external control input, set by the resistors 1 k Ω , 33 k Ω and the 10 k Ω potentiometer, as shown in Fig. B.1. After the DAQ analog output is given to the magnet control circuit, the program waits for 400 ms. The wait time is defined by the data reading rate of the FLUKE 8840 multimeter, and is 342 ms in “slow reading rate” mode.

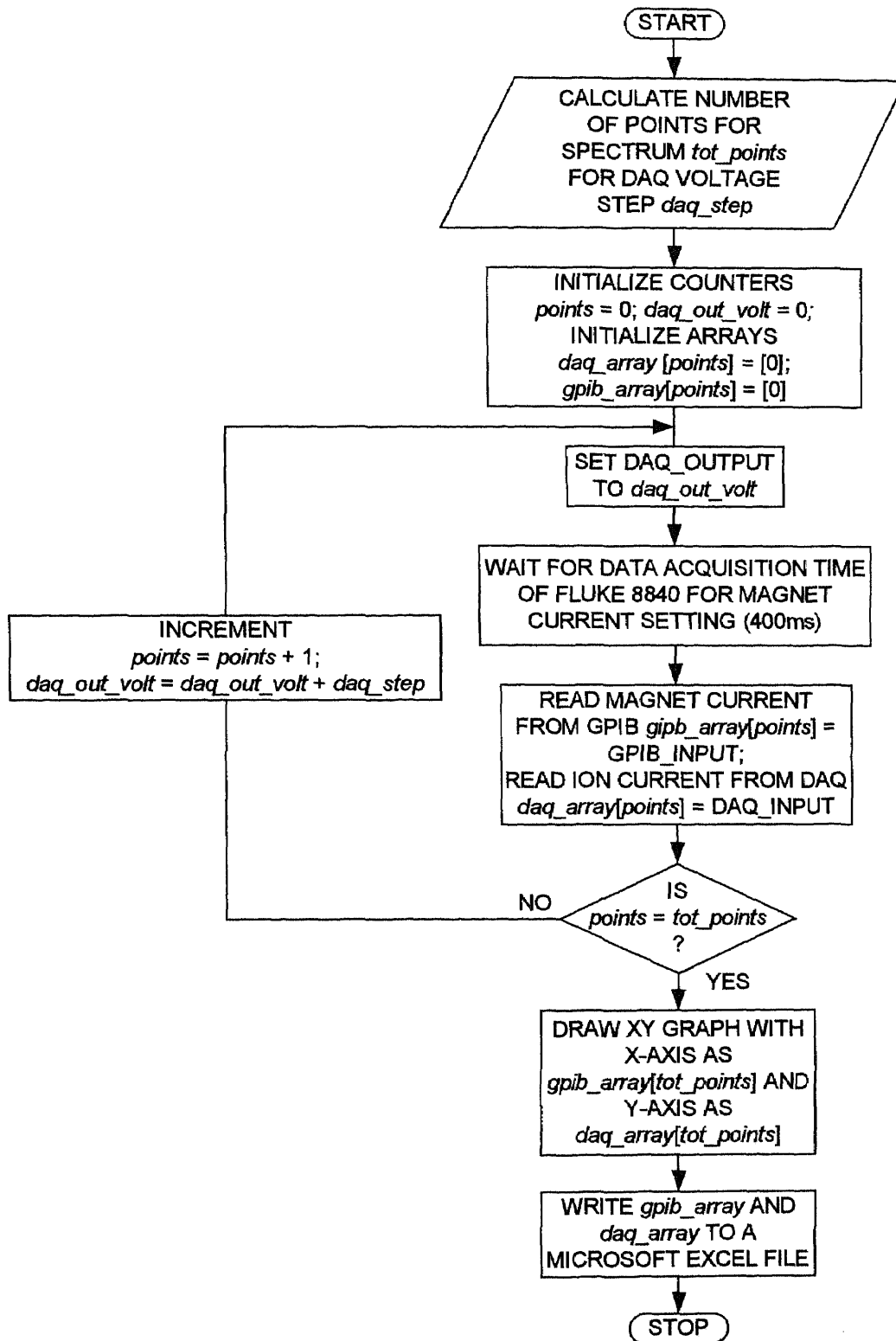


Fig. B.3 Flowchart for Data Acquisition and Control

Then, the magnet current and the ion current are read and stored in arrays. If the total number of points has not been reached, the magnetic field is incremented and the process is continued. Once the set number of points is completed, an x-y graph is drawn and the values of x and y arrays are stored as a spreadsheet file for analysis.

Fig. B.4 shows the front panel for the ion current spectrum VI file. The inputs to the program are located at the top row and the outputs are displayed at the bottom row.

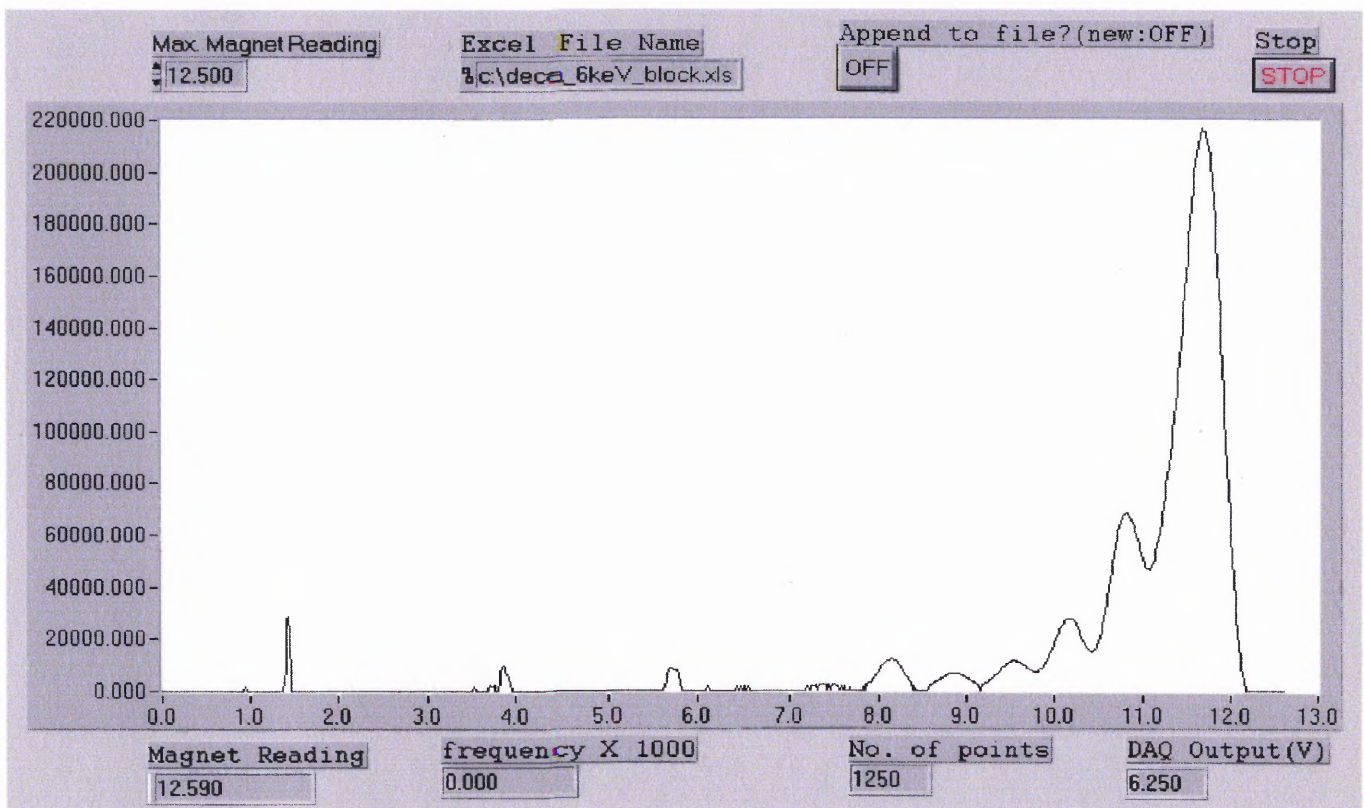


Fig. B.4 Front Panel of LabVIEW™ Program for Ion Spectrum

The “Max. Magnet reading” input is used to set the maximum magnet setting, upto which the spectrum is to be obtained. Typical values for the maximum magnet setting are 8.75 for argon at 9 keV (since the peak is observed at 8.25) and 10.00 for decaborane at 4 keV (since the peak is observed at 9.35). The name of the file, in which the resulting spectrum

is to be stored, is entered in the field “Excel File Name”. An option for appending to an existing file is provided. The maximum magnet setting and the output file name are entered before running the program. After the total number of points for the spectrum is obtained, the spectrum is displayed on the x-y graph in the center field of the front panel and the program execution stops. The “Stop” button is pressed and the program is executed to gradually reduce the magnet current to zero.

The first field at the bottom row displays the current magnet reading and the second field displays the frequency from the ORTEC 439. These values change for each point acquired during program execution. The third field displays the calculated number of points for the spectrum, which is constant. The fourth field displays DAQ output voltage, which controls the magnet current, and changes for each point acquired during program execution.

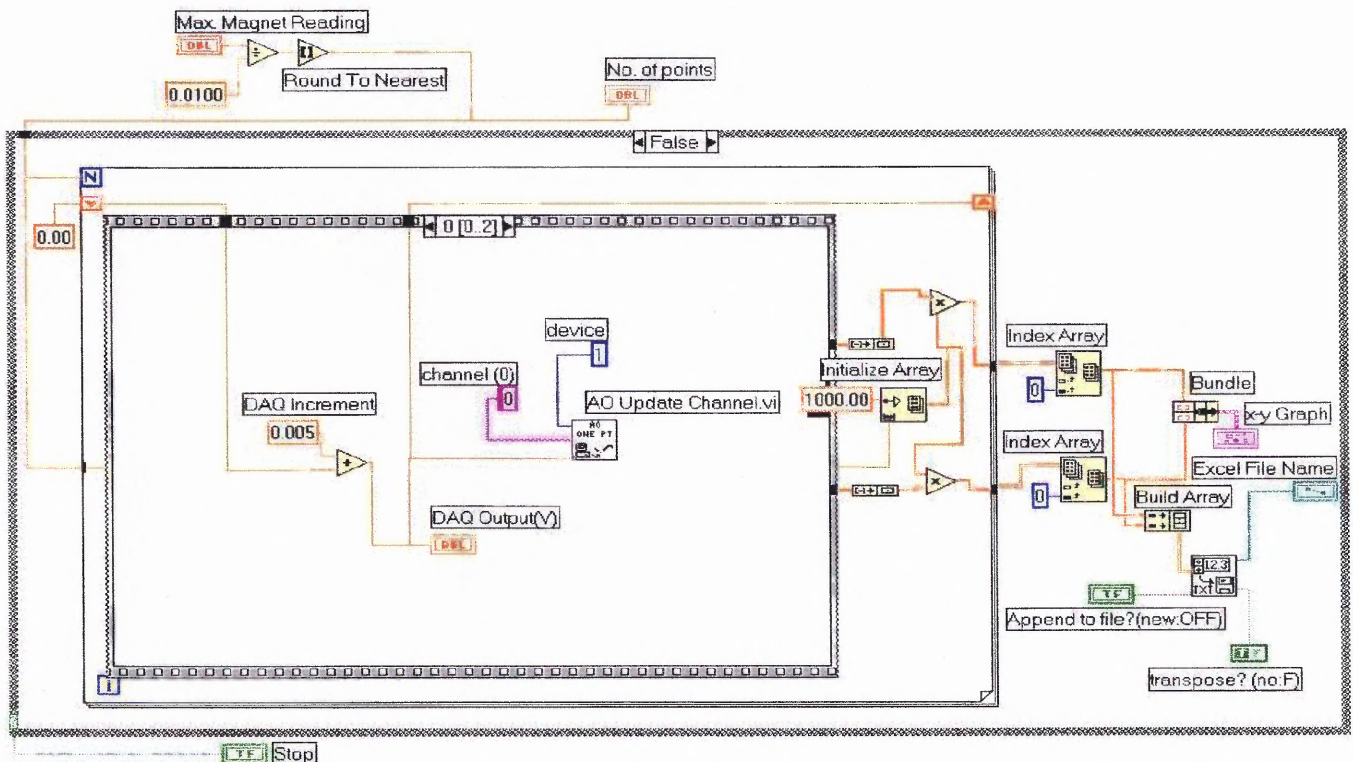


Fig. B.5 Functional Block Diagram-DAQ Analog Output (AO Update Channel)

Fig. B.5 shows the section of the functional block diagram corresponding to the first sequence of execution of the program where the analog output is generated by the DAQ board for the magnet control. The main function used here is the “AO Update channel” that outputs an analog voltage to a given channel. This function accepts three parameters namely the DAQ device address, the channel used and the value of the DAQ output voltage. A shift register, which is initialized to zero, is used to store DAQ output voltage values from previous loop iterations and is incremented by 5 mV in each iteration of the “for-loop”.

Fig. B.6 shows the second sequence where the “wait” function is used to wait for the FLUKE 8840 data acquisition time of 400 ms in the “Slow Data Rate” mode.

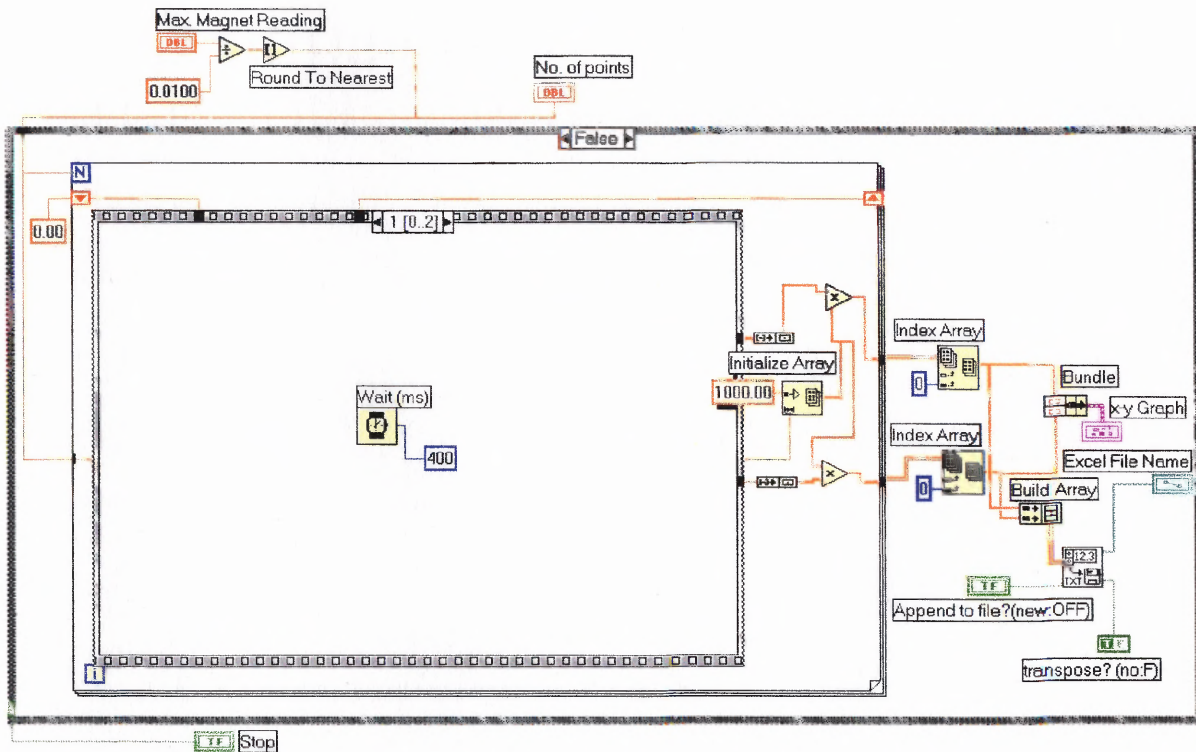


Fig. B.6 Functional Block Diagram-Wait Function

Fig. B.7 shows the third sequence where the “GPIB Read” function and the pre-defined sub-vi file “Measure Pulse Width or Period.vi”, are executed simultaneously. The “GPIB Read” function is used for obtaining the reading of the FLUKE 8840. The function “Measure Pulse Width or Period.vi” sub-vi file is used for obtaining the pulse width of the digital signal that is connected to the GATE pin of one of the DAQ counters. The “time limit” parameter for this sub-vi specifies the maximum time for acquisition of one pulse by the DAQ counter. This value in turn decides the minimum ion current that is read. The parameters “device” and “counter” give the address of the DAQ card and the counter that is used. The fourth parameter is the type of pulse width measurement to make, as given below:

Value 0: Pulse width from rising to falling edge.

Value 1: Pulse width from falling to rising edge.

Value 2: Period between adjacent rising edges. (default)

Value 3: Period between adjacent falling edges.

The default value 2 is used in the program. The output value of pulse width from this sub-vi file is used to obtain the frequency of the input signal, which is proportional to the ion current. The frequency is multiplied by 1000 before it is stored in an Excel file to avoid truncation errors. A predefined “From Exponential/Fract/Eng.vi” file is used to convert the GPIB string output to a numeric value before it is stored in the Excel file.

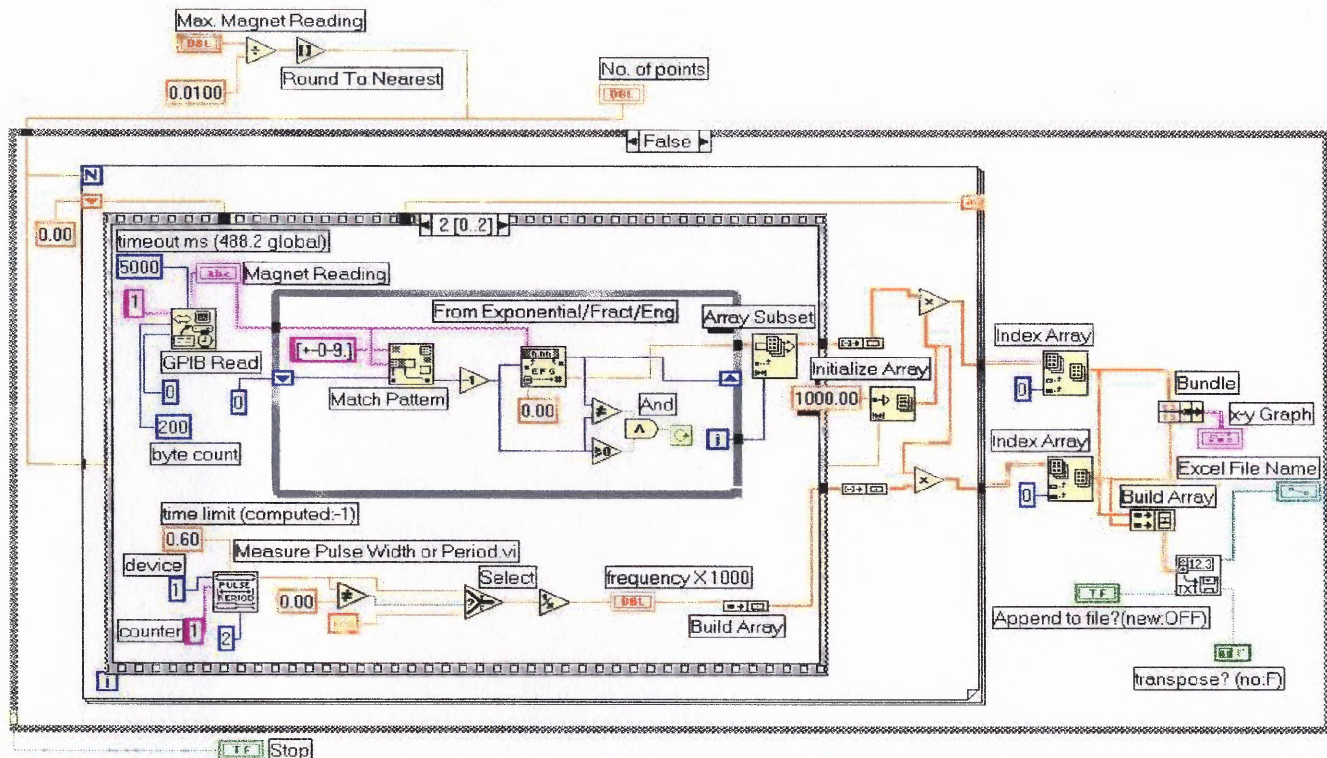


Fig. B.7 Functional Block Diagram-DAQ Read (Measure Pulse Width) and GPIB Read

B.3 Dose Control

The electronics for ion current and dose measurements includes EG & G ORTEC 439 Digital Current Integrator and EG & G ORTEC 871 Timer. Both instruments obtain operating power from a Nuclear (NIM) Standard Bin and Power supply. The EG & G ORTEC 439 Digital Current Integrator is used to integrate the ion current on the sample. It is designed to accurately measure direct current or the average value of pulse currents, such as accelerator beam currents, and digitizes the input current by producing an output pulse for specific values of input charge. There is a selection switch with three settings for the amount of charge (10^{-10} , 10^{-8} or 10^{-6} coulomb) required to produce an output pulse [19]. This switch is used in combination with a multiplier switch to set the full-scale

reading of the ORTEC 439 to measure input current. The instrument is normally in standby when it is powered on or when any other selector settings are changed. The “Test Current” setting on the selector switch produces a digital output of ~1 kHz on each coulomb/pulse setting. The instrument is set to “Operate” during measurements.

The EG & G ORTEC 871 Timer and Counter is used to count the pulses that are output from the current integrator [20]. The ORTEC 871 is a modular general-purpose instrument that includes an 8-decade counter, an 8-decade presettable counter (called timer) and a time base. The presettable portion is used as a counter, which counts pulses from the ORTEC 439. The number of pulses to be counted is set by using pushbuttons INC M and INC N to achieve a preset value of $M \times 10^N$. The time base select switch is set to “Ext” for this mode. At the same time, the nonpresettable portion of the instrument counts 0.1-second pulses that are furnished from the internal time base. The display can be switched to display the counts from the timer or the counter by using the select pushbutton.

The ORTEC 439 is calibrated for the ranges 10^{-10} coulomb/pulse for ion currents of the order of hundreds of nanoamperes and for 10^{-8} coulomb/pulse for ion currents of the order of tens of microamperes. The ORTEC 871 is set to count the required number of pulses for a given dose and implant area given by the formula

$$c = \frac{\phi A q}{S} \quad (\text{B.1})$$

Where : c is the number of counts

ϕ is the dose in ions/cm²

q is the electron charge in coulombs

A is the implant area in cm^2

s is the coulomb/pulse setting on the ORTEC 439 current integrator

The time of implant can be obtained from the nonpresettable counter and verified by using the formula:

$$t = \frac{nq\phi A}{I} \quad (\text{B.2})$$

Where : t is the time of implant in seconds

I is the ion current in amperes

n is the charge state on the ion

REFERENCES

1. "The National Technology Roadmap for Semiconductors", *Semiconductor Industry Association, 1994*.
2. Peter Singer, "Ion Implanters: Pushing the Low Energy Limits", *Semiconductor International*, pp. 72-78, April 1996.
3. Ruth De Jule, "Meeting the Ultra-Shallow Junction Challenge", *Semiconductor International*, pp.50-54 April 1997.
4. Marek Sosnowski, "The Prospects for Low Energy Implantation with Large Molecular Ions-the Case of Decaborane, *The American Institute of Physics*, College Park, MD 20740 pp.775-778, August 1999.
5. Cheung, N.W., En, Jones, E. and Yu, C., "Plasma immersion ion implantation of semiconductors", *Mat. Res Soc.Symp.Proc.279*, 297 (1993).
6. Goto. K, Matsuo, J.Sugii, Isao Yamada and T.Hisatsugu, "Novel Shallow Junction Technology using decaborane ($B_{10}H_{14}$)", *IEDM-96, IEEE*, pp.768-771, 1997.
7. Sosnowski, M., Gurudath, R., Poate, J., Muijsce, A., Jacobson, D., "Decaborane as Ion Source Material for Boron Implantation", *Mat. Res Soc. Symp. Proc*, pp.49-54, Vol 568, 1999.
8. Ken-ichi,Goto, Jiro Matsuo,Yoko Tada, Tetsu Tanaka, Youichi Momiyama, Toshihoro Sugii, and Isao Yamada, "A High Performance 50nm PMOSFET using Decaborane ($B_{10}H_{14}$) Ion Implantation and 2-step Activation Annealing Process," *IEDM-97, IEEE*, pp. 18.4.1-18.4.4, 1997.
9. Jiro Matsuo, Daisuke Takeuchi, Takaaki Aoki and Isao Yamada, "Cluster Ion Implantation for Shallow Junction Formation," *IEEE*, pp. 768-771, 1997.
10. Gurudath, Ravidath, "Development of an Ion Source for Implantation of Decaborane", *Master's Thesis, January 1999*, Dept. of Electrical and Computer Engineering, New Jersey Institute of Technology, Newark, NJ 07102.
11. Ian.G.Brown, *The Physics and Technology of Ion Sources*, John Wiley & Sons, NY, 1989.
12. F.Shoji and T.Hanawa, "Ion source constructed from Ionization gauge," *J.Phys.E: Sci.Instrum*. Vol.14, pp. 1721-24, 1981.

13. J.Kirschner, "Simple low-energy sputter ion gun based on a Bayard-Alpert pressure gauge," *Rev. Sci. Instrum.*, vol. 57, pp.2640-2642, 1996.
14. *Kimball Physics eV Parts Manual*, Kimball Physics Inc., Wilton, NH 03086.
15. David A. Dahl, *SIMION 3D Version 6.0 user's Manual*, Idaho National Engineering Laboratory Idaho Falls, ID 83415, 1995.
16. Campbell, Stephen A., *The Science and Engineering of Microelectronic Fabrication*, Oxford University Press, 198 Madison Avenue, NY 10016, 1996.
17. G. Dearnaley, J.H. Freeman, R. S. Nelson, and J. Stephen, *Ion Implantation*, New Holland Amsterdam, 1973.
18. *Operating and Service Manual, Regulated DC Power Supply HP Models 6259B, 6260B, 6261B, 6268B, 6269B*, Hewlett Packard Inc. Roakville, MD 20850.
19. *Operating and Service Manual, Digital Current Integrator, Model 439*, EG & G Inc., Oak Ridge, TN 37831.
20. *Timer and Counter Instruction Manual, Model 871*, EG & G Inc., Oak Ridge, TN 37831.
20. National Instruments URL <http://www.ni.com/labview/what.htm> (Dec. 29, 1999).
21. National Instruments URL <http://www.ni.com/labview/basics.htm> (Dec. 29, 1999).
22. *DAQ PCI E Series User Manual, Multifunction I/O Boards for PCI Bus Computers*, National Instruments Corporation, Bridge Point Parkway, Austin, TX 78730.
23. *GPIB NI-488.2MTM Function Reference Manual for Win32*, National Instruments Corporation, Bridge Point Parkway, Austin, TX 78730.
24. Hurd, T.Dallas, *An Introduction to the Chemistry of the Hydrides*, Wiley NY 1952.
25. Bishop, Robert H., *Learning with LabVIEW*, Addison Wesley Longman Inc., 2725 Melno Park, CA 94025.